On-Line Grasp Estimator: A Partitioned State Space Approach [1]

Rod Grupen, Jefferson Coelho, and Kamal Souccar

Laboratory for Perceptual Robotics
Department of Computer Science
University of Massachusetts

Technical Report #92-75
October, 1992

Abstract

This paper reports preliminary results of work focused on reflexive and reactive controllers for managing a 20 degree-of-freedom (DOF) hand/arm system performing grasping tasks. The goal is to provide a framework for sensor-based controllers that acquire visual and haptic information on-line and use this data stream to refine grasping solutions. We will present several such behaviors and illustrates how they can be used to suppress local errors in the neighborhood of a grasp solution.

[1] This work is supported in part by NSF CDA-8922572 (CII), IRI-9116297, IRI-9208920 (CRICCS), and CNPq 202107/90.6

Contents

1 Introduction

A great deal of work has focused on developing cooperative and dextrous manipulation systems. This domain is composed of independently challenging issues: dimensionality, redundant degrees of freedom, uncertainty resolution in modeling, planning, and execution.

1.1 Dimensionality

The "find-path" problem for configuration spaces obstructed by polynomially described boundary (given perfect information) has already been completely solved by Schwartz and Shahir[40]. A nearly optimal solution has been suggested by Canny for this class of problems as well[8]. However, combinatoric algorithms for finding a path with algebraic constraints are exponential in the number of degrees of freedom (DOF) in the system[8].

Moreover, "complete" process models are expensive to build. Detailed plans for grasping which are beyond the limits of model certainty and reliability are of little value, consume scarce system resources, and may subsequently require significant replanning. The active sensing paradigm addresses these perceptual expenses by directing sensory resources to important features of the process. Various objectives to direct the sensing strategy have been proposed, among these: model acquisition [1, 2, 3, 42], grasping[3, 21], recognition[13, 18, 23], gaze fixation[4], and navigation[16]. Since these techniques attempt to determine *what* information is necessary and *when* it is required, they couple the control problem to the perceptual problem. The evaluation can be accomplished by executing a control hypothesis and actively resolving inconsistencies between the model and observation. The incremental control hypothesis constitutes an active, *control-based* model revision.

Complexity and dimensionality issues have led to behavior-based system architectures. In this paradigm, complex state spaces are decomposed into tractable subspaces which form a basis for all system behaviors [5, 6, 19, 38]. This *factorization* greatly enhances run-time performance. For example, the subsumption architecture[5, 6] and Raibert's hopping platforms[38] partition a complex state space into disjoint controllers that are activated by sensory events. It has been demonstrated that this approach can be used to generate controllers for rather complex processes.

The system we propose incorporates *behaviors* (controllers designed to optimize particular performance criteria) to regulate the state of the process. Elements of the suite of behavior are activated in a competitive scheme in which a task (conjunction of sub-goals), the local gradient of the performance indices, and the ability of the robot to address each gradient is considered. The objective of this work is to discover a means of modulating control such that incremental evidence and the current environmental context can continually adjust the solution strategy.

1.2 Redundancy Resolution

Analogous to this behavior-based control methodology are the pseudoinverse-based techniques aimed at exploiting redundant degrees of freedom in a robot mechanism. This work establishes a prioritized set of behaviors in the form of performance indices and attempts to address low priority sub-goals of the task in the null space remaining after the solution of high priority sub-goals. Conditioning metrics for redundant manipulators have been used as a design tool for relating a manipulator to a task domain[39], as scalar objective fields for optimizing the inverse kinematic solution [9, 10, 27, 29, 30, 33, 47, 48].

The performance metric is used to discriminate between competing configurations in a redundant manip-

ulator. For example, Yoshikawa employs a pseudoinverse (least-squares) solution to the inverse kinematics problem with two forms of second priority configuration objectives[47]. The controller is expressed as:

$$\dot{\theta} = J^{+}\dot{x} + (I - J^{+}J)\kappa \tag{1}$$

where κ is an *internal* or null space motion which optimizes a performance metric:

$$\kappa = K\frac{\partial p}{\partial \theta}. \tag{2}$$

The first *priority* task in the control expressed by Equation 1 is the Cartesian velocity command. If the redundant manipulator has excess degrees of freedom, then the posture is adjusted to optimize the secondary preformance metric, p.

In this literature, researchers have focused primarily on optimizing the posture of the robot during the execution of a Cartesian trajectory. The performance metrics reported include:singularity avoidance, manipulability, obstacle avoidance, postural bias, inverse kinematic accuracy and feasibility, and the compatibility of manipulator posture with task specified forces and velocities. Multiple, prioritized performance specifications can be addressed in a uniform manner. However, the relationship between the behavior produced in such a system and the behavior specified in the controller design is not clear. The behavior that emerges from the controller depends directly on the null space preserved after the indulgence of higher priority performance metrics. The performance of the system with respect to any of these criteria varies with the manipulator Jacobian.

1.3 Reasoning in the Force Domain

Considerable progress in grasp planning has been published in the 1980's. The Grip Transform was developed to express the transformation from a set of contact forces or velocities to a net object frame force or velocity[32, 39]. Mathematical programming techniques employing frictional constraints have been described to formulate the grasp force solution[20, 26, 33]. The computed torque control technique has been augmented to include object dynamics and internal grasp forces so that object position and orientation can be regulated within the workspace of the hand[28]. The quantitative formulation of a force closure grasp[36] and the effective stiffness of the grasp provides a means of comparing grasp configurations to task specifications[37]. Researchers have also investigated the use of contact geometry ("liftability"[45]) for grasp formation, and friction and compliance to generate object reorientations in 2D[15, 31].

The problem of designing the grasp configuration has also received a good deal of attention. Results have been reported for several "knowledge-based" grasp planners. Fast geometric algorithms for finding force closure contact geometries for polygonal (planar) objects have developed [37] and have been extended (to significantly slower algorithms) for two contacts on piecewise polynomial planar objects[14]. Other work derives grasp controllers from human grasp taxonomies[12, 24, 35, 44]. We refer to this perspective as "knowledge-based" because they rely to a large degree on complete geometric information about the world in the first case, and because they rely on emulating human grasps in the latter case. Moreover, taxonomy-based controllers require multiple sensorimotor mappings to express alternative manipulation tasks. The resulting "*exponential cortex*" may not be a viable control architecture for highly redundant, general purpose systems.

Grasping has also been approached as an optimization problem. Jameson and Leifer describe a system which optimizes a grasp goal function[25]. Artificial potential fields which avoid first order slip conditions and which penalize unfavorable contact geometries are superimposed to generate a search space. These potential fields penalize contacts near the tip of the finger, the palm, contacts near the table top, and finger configurations with extreme joint angles. This work also requires complete geometry. Our approach decouples the hand and the object — reducing the complexity of the state space. Moreover, we proposed

to control grasp formation on the basis of incomplete geometry. Jameson and Leifer noted that geometric smoothing should simplify the optimization problem. We are investigating smooth models in the force domain which are also convex.

2 Sensorimotor Behavior Design Specification

2.1 Reflexive, Reactive, and Deliberative Behavior

For the sake of discussion, we have adopted a nomenclature for distinguishing three forms of behavior in terms of the computational complexity and the source and scope of knowledge employed by the controller.

Reflexive behaviors are *hardwired* encapsulations of behavior. Biological organisms develop *light-weight* transformations computed on the basis of local stimulation, the local connectivity of the peripheral nervous system, and the musculoskeletal configuration. Prototypical examples include the human grasp reflex which appears for a short period in the first year of infant development, and the plantar reflex in human gait control. This form of behavior is event driven and characterized by very tight sensor-effector arcs. There is no persistence or interpretation of the sensory information.

Reactive behavior differs from reflexive behavior in its capacity to incorporate new information, perhaps extending or modifying the current context. In this sense, reactive behavior is based on more global information accumulated in persistent models rather than on local sensory information exclusively. These behaviors permit the continuous deformation of control surfaces and thus allows the data stream to modulate individual behaviors of the system and the composition of behavior.

Deliberative behavior requires relatively complete information about the world, and it uses this knowledge to predict the sequence of future states of the system. This prediction permits the system to compare the future consequences of all candidate actions and to optimize the system performance. A fundamental issue facing the designers of deliberative behavior is the non-stationary nature of the world, and that the process of observation itself is prone to error. This implies that, in general, all deliberative behavior must involve some degree of risk.

Perhaps the most compelling justification of reflexive and reactive behavior, is the property of *local, bounded error suppression* and its value to deliberative behavior. When the state of the world is not quite what it appears we may rely to some extent on reflexive and reactive behavior to suppress deviations between our models and reality. Reactive systems may be able to find solutions to simple problems in complex environments. Moreover, they may be capable of occasionally stumbling onto very good solutions. However, to increase the probability of a favorable outcome, these experiences must be fused over time and a deliberative agent must be devised to exploit this increasingly global information. In this sense, deliberative behavior can be used to position the reactive subsystems *upstream* of a particularly robust solution to a specific problem — relying on the local competence of these reactive systems to attain the goal with no further cognitive expense.

2.2 Declarative Behavior

Reflexive behavior must be formulated in light of specific sensors and mechanisms to be useful. They express procedural responses to fundamental constraints in the system and exploit particular kinematic and computational structures in the mechanism. Brooks' subsumption architecture precompiles the structure of the robot, the range of environment, and the task domain into a hardwired, procedural repertoire. Environments which are not anticipated cause these precompiled strategies to fail. Likewise, broad ranges of

tasks may require mutually exclusive behaviors which cannot be selected solely on the basis of instantaneous sensor information.

This work attempts to capture the *quality* of successful interaction with the world in the form of a set of declarative behaviors. This behavioral specification permits the on-line compilation from resources, tasks, and environment into an instance of a procedural solution. Our goal is to produce substantially more flexibility in the response of the system to novel circumstances. The reactive grasp controller we describe is declarative in the sense that sub-goals are expressed in a task/device independent manner. One behavior controls the configuration of contacts which collectively produce wrench closures. This metric space is modulated by observing object geometry in the process of executing a grasp. Another behavior controls the posture of the mechanism allocated to the task by analyzing the relevant manipulator Jacobians.

2.3 Relationship to Psychological Models

There is a similarity between the notion of *behavior* employed in this approach to robot control and the composition of control observed by psychologists observing the development of reaching and grasping behavior in humans[7, 43]. Bruner cites *constituent acts* [7] and Thelen observes certain *component abilities* [43] defined as motoric actions, that are not necessarily independent or adequate for all situations. In both these studies, behavior (or the soft-assembly of heterogeneous component abilities) is constructed for a specific purpose or task. Our approach is motivated by the same computational issues as were postulated by Thelen, i.e., that component abilities are necessary to overcome the incredible complexity involved in combining the available resources. The same complexity forbids the existence of pre-defined procedures or prefigured patterns of behavior. The maturation process described by both Bruner and Thelen is proposed as a mechanism by which constituent acts are composed to yield solutions to the broad domain of manipulation tasks given the perceptual context. A hypothesis common to both the psychological literature and the approach proposed here is that there can be a limited set of behaviors whose collective response is modulated by the current world state.

A significant difference to the human developmental sequence exists as well. In the first year of development, humans acquire coarse-motor skill (reaching), followed by fine-motor skills, culminating in the ability to perform dextrous, fingertip manipulation. During this year, the infant also acquires experience with objects in the world and begins to associate these forms with function. This concurrent motor — cognitive development is absent in our controllers. We have expressed relatively rich strategies for fine-motor control in the robot behaviors rather than learning these strategies from experience, consequently, our robot knows *how* to address certain tasks, but it doesn't have the slightest clue *why*. This knowledge is almost certainly required to make effective use of a dextrous machine. It is fair to assume that purely reactive dextrous grasp controllers can't hope to respond to the breadth of manipulation contexts without exploiting knowledge-based constraints.

3 The "Grasp" Problem

In this work, a **contact configuration** is defined as a hand/arm configuration and a contact geometry which transmits contact wrenches to the object via the surface geometry. The goal is to decompose this complex planning problem into decoupled controllers which independently regulate aspects of the planning problem and to compose a solution from these constituent controllers.

A grasp solution is **stable** if the contact configuration is capable of rejecting arbitrary perturbation forces. This requires that external wrenches can be supressed by contact wrenches derived from normal and frictional contact forces. Stability is enhanced when contact forces are evenly distributed over the contacts[34].

A grasp configuration can be designed to effectively apply **task specific wrenches** to the object. A grasping task is described in the force domain by specifying a set of wrenches (forces and torques) relative to an object coordinate frame. In this work, we will address n-fold, rotationally symmetric, convex object geometries.

The approach reported in this paper, refines a grasp estimate by iteratively descending a composite error surface in toward the nearest "optimal" contact configuration. Performance indices (and associated error surfaces) are derived from models of the object geometry and from manipulator kinematics. Such models can exhibit many local minima (see Figure 2). We will describe heuristic control surfaces based on smoothed force domain models and on locally planar surface geometries. The former is used to solve for a force closure grasp while avoiding many local minima. The latter is used to refine the resulting contact geometry for this class of objects. This control surface yields moment closure grasps in the vicinity of approximate force closure grasps. The grasp synthesis process manipulates the placement of frictionless point contacts in the contact configuration space. We will consider the placement of qualitative, normalized contact forces on the object's surface. This representation characterizes the ability of the geometric surface to transmit task specific contact wrenches. A third controller is described that regulates the hand configuration with respect to the manipulability metric. Behavior compositions are employed as iterative estimators on a family of observed error surfaces.

3.1 Controlling a Grasp Geometry in the Force Domain

Given a contact geometry with associated contact models, the set of forces on the surface of an object,

$$\mathbf{F} = \{\vec{f} | \vec{f} \in R^n\}, \tag{3}$$

maps to a set of object frame wrenches,

$$\mathbf{W} = \{\vec{w} | \vec{w} \in R^m\}, \tag{4}$$

$$\mathbf{W} \subset R^m, \tag{5}$$

using a linear mapping $\mathcal{G}$. If we restrict ourselves to the case where no contact torques are applied to the object's surface, then the mapping is defined by Equation 6.

$$\begin{aligned} &\mathcal{G} : R^n \mapsto R^m \; \textit{such that} \\ &\mathcal{G}(\vec{f}_i) = (\vec{f}_i, (\vec{r}_i \times \vec{f}_i)) \\ &\mathcal{G}(\mathbf{F}) = \mathbf{W} \end{aligned} \tag{6}$$

where $\vec{r}$ is the position vector of the contact location relative to the task frame.

Grasp stability requires that the union of the wrench subspaces generated by the contact system and external forces must span six dimensions. If this condition is met, infinitesimal perturbations of the object may be resisted by forces generated in the manipulator and/or environment. The robustness of this stability is related to the magnitude of perturbations that the contact system can resist.

The subsequent discussion will make use of the following nomenclature.

$\vec{\omega}_i$ a particular wrench space vector resulting from the i^{th} interaction force.

W_i the set of normalized wrenches applied at the i^{th} contact position.

$\mathbf{W} = [W_1\ W_2\ \ldots\ W_n\ ]$, is the *Grasp matrix.*

We will refer to the wrench derived from the force along the surface normal as an *independent* wrench, and the wrench derived from an associated tangential contact force as a dependent wrench.

Figure 1 illustrates a two contact grasp configuration. This system of forces produces a corresponding

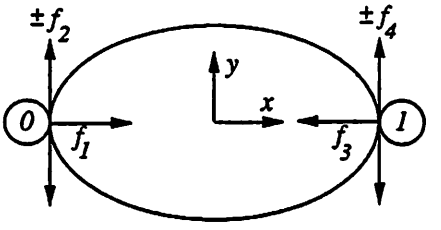

Figure 1: A Grasp Geometry

system of wrenches at contact positions 0 and 1. These wrenches are recorded columnwise in the W matrix shown in Equation 7.

$$\mathbf{W} = [\, W_0^T \mid W_1^T \,] = \begin{bmatrix} 1 & 0 & -1 & 0 \\ 0 & 0.707 & 0 & 0.707 \\ 0 & 0 & 0 & 0 \\ 0 & 0 & 0 & 0 \\ 0 & 0 & 0 & 0 \\ 0 & -0.707 & 0 & 0.707 \end{bmatrix} \tag{7}$$

The span of W can be identified by computing the singular value decomposition of grasp matrix.

$$\mathbf{W} = U\Sigma V$$

The result of the SVD of the grasp matrix, Equation 7, yields;

$$\Sigma = diag[1.414,\ 1.0,\ 1.0,\ 0.0]$$

$$U = \begin{bmatrix} -1 & 0 & 0 & 0 \\ 0 & 1 & 0 & 0 \\ 0 & 0 & 0 & 1 \\ 0 & 0 & 0 & 0 \\ 0 & 0 & 0 & 0 \\ 0 & 0 & -1 & 0 \end{bmatrix} \qquad V = \begin{bmatrix} -0.707 & 0 & 0 & -0.707 \\ 0 & 0.707 & 0.707 & 0 \\ 0.707 & 0 & 0 & -0.707 \\ 0 & 0.707 & -0.707 & 0 \end{bmatrix} \tag{8}$$

There are three nonzero singular values which define the rank of the contact system to be three. Correspondingly, the first three column vectors in U define the space spanned by the contact system. U (Equation 8) shows that this grasp configuration can apply restorative forces in the $-\hat{f}_x$ and $\hat{f}_y$ directions and a restorative moment about the z axis, $-\hat{m}_z$. The forth column vector in V identifies the null space of the system. A null space combination of contact wrenches may be scaled up arbitrarily without producing a net external wrench on the object. Therefore, the family of such solutions is:

$$\lambda\, [\, -0.707\hat{w}_1 \; - \; 0.707\hat{w}_3], \; (\lambda < 0). \tag{9}$$

3.1.1 Sufficient Grasp Geometries

The criteria we will employ for a stable grasp configuration is the construction of a *null space* within the grasp matrix (Section 3.1).

Principle 3.1 (Null Space Sufficiency) *If a null space can be constructed from a set of independent wrenches, $\{\omega\}_n$, derived from normal contact forces, then a grasp wrench, ω_{ext} within the wrench space spanned by these normal wrenches and their associated frictional wrenches, $\{\omega\}_{ext} \in span(\{\omega_n\} \bigcup \{\omega_f\})$, can be executed through an appropriate linear combination of contact wrenches.*

This observation is valid for three dimensional objects and two or more soft finger contacts or for 3 or more point contacts with friction. Extensions of this approach are required in order to take advantage of lower order contact constraints and/or compound contact types. Given these assumptions, if wrenches derived from frictional forces are insufficient for the task, the object can be *squeezed* within the null space until ω_{ext} is achieveable. This observation establishes an equivalence class of sufficient contact geometries which can meet force domain specifications [21, 41].

The null space condition can be expressed by a quadratic form based on a normalized residual wrench vector, ρ.

$$\begin{aligned} \epsilon_S &= \vec{\rho}^T \vec{\rho} \\ &= \left(\vec{t} - \frac{1}{n}\sum_{i=1}^{n} \hat{\omega}_i\right)^T \left(\vec{t} - \frac{1}{n}\sum_{i=1}^{n} \hat{\omega}_i\right) \end{aligned} \tag{10}$$

where $\vec{t}$ is an optional wrench closure *bias*, and the residual wrench vector, $\vec{\rho}$, expresses the net wrench over $1 \leq j \leq n$ contacts. The elements, $t_j \in [-1, 1]$, of $\vec{t}$ and the elements, $w_{ij} \in [-1, 1]$ of $\vec{w}_i$ are qualitative in the sense that they do not reflect engineering units of force and torque, but express the relative ability of a contact configuration to transmit forces and torques through the object's surface. That is, the maximum(minimum) force/moment applied to the object by a single contact is $+1(-1)$. The solution contact configuration is an optimization based on shape rather than dimension. Equation 10 is zero iff there exists an equivalent linear combination of contact wrenches, $\vec{t} = (1/n)\sum \hat{\omega}_i$ for wrench task, $\vec{t}$.

Differentiating Equation 10 with respect to θ_i yields:

$$\begin{aligned} \frac{\partial \epsilon_S}{\partial \theta_i} &= 2\left(\vec{t} - \frac{1}{n}\sum_i \hat{\omega}_i\right)^T \frac{\partial\left(\vec{t} - \frac{1}{n}\sum_i \hat{\omega}_i\right)}{\partial \theta_i} \\ &= -2\left(\vec{t} - \frac{1}{n}\sum_i \hat{\omega}_i\right)^T \frac{\partial \omega_i}{\partial \theta_i}\frac{1}{n} \\ &= -\frac{2}{n}\vec{\rho}^T G_i \\ &= -\frac{2}{n} G_i^T \vec{\rho}, \end{aligned} \tag{11}$$

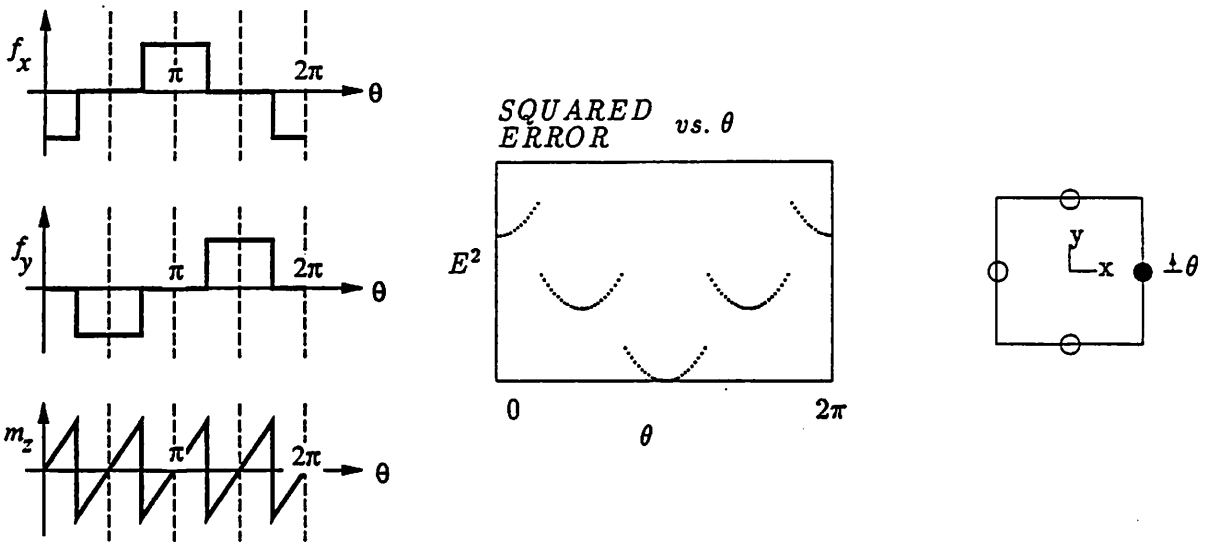

Figure 2: The Force Model, the Sufficiency Metric ($\vec{t} = \vec{0}$), and the Attractors for the Square

and, therefore,

$$\frac{\partial \epsilon_S}{\partial \vec{\theta}} = -\frac{2}{n}\begin{bmatrix} G_1^T \\ G_2^T \\ \vdots \\ G_n^T \end{bmatrix}\vec{\rho} = -\frac{2}{n}G^T\vec{\rho}. \quad (12)$$

Equation 12 evaluates to $\vec{0}$ in one of two circumstances;

(a) $\vec{\rho} = \vec{0}$, and

(b) when $\vec{\rho}$ is orthogonal to G^T such that $G^T\vec{\rho} = \vec{0}$.

The first condition is the desired convergence criterion and results in a grasp geometry that can be *scaled* (in the sense of Principle 3.1) to span the task. The second criterion is equivalent to a local minimum in the control surface. This class of attractors results when a local tangent to the wrench surface, G, is orthogonal to the residual vector, $\vec{\rho}$. A simple example of this phenomena is when a single contact is placed on a circle (sphere) with task bias wrench, $\vec{t} = \vec{0}$. Here the contact wrench, $\vec{\omega}$, is orthogonal to the derivative wrench, $\partial\vec{\omega}/\partial\theta$.

Figure 2 demonstrates these two types of equilibrium grasp configurations. This figure illustrates the wrench functions, $f_x(\theta)$, $f_y(\theta)$, and $m_z(\theta)$, the error surface, and the positions of attractors in the metric space for a square shape. In this figure, a contact is located at $\theta = 0$ (solid circle) and the error surface is used to regulate the position of the second contact. Both contacts are modeled as frictionless point contacts. The moving contact will migrate toward one of four separate attractors in the error metric depending on the initial configuration. Of these equilibrium grasp configurations, only the global minimum is sufficient.

The other minima are generated at contact locations where the local wrench gradient, G, is orthogonal to the residual vector, $\vec{\rho}$.

The Hessian of Equation 10 is in the form:

$$\begin{bmatrix} \frac{\partial^2 \epsilon}{\partial \theta_1^2} & \frac{\partial^2 \epsilon}{\partial \theta_1 \partial \theta_2} & \cdots & \frac{\partial^2 \epsilon}{\partial \theta_1 \partial \theta_n} \\ \frac{\partial^2 \epsilon}{\partial \theta_2 \partial \theta_1} & \frac{\partial^2 \epsilon}{\partial \theta_2^2} & \cdots & \frac{\partial^2 \epsilon}{\partial \theta_2 \partial \theta_n} \\ & & \vdots & \\ \frac{\partial^2 \epsilon}{\partial \theta_n \partial \theta_1} & \frac{\partial^2 \epsilon}{\partial \theta_n \partial \theta_2} & \cdots & \frac{\partial^2 \epsilon}{\partial \theta_n^2} \end{bmatrix} \tag{13}$$

The diagonal terms of the Hessian look like:

$$\begin{aligned} \frac{\partial^2 \epsilon}{\partial \theta_i^2} &= -\frac{2}{n}\left[\frac{\partial G_i^T}{\partial \theta_i}\vec{\rho} + G_i^T \frac{\partial \vec{\rho}}{\partial \theta_i}\right] \\ &= \frac{2}{n}\left[\frac{G_i^T G_i}{n} - \frac{\partial G_i^T}{\partial \theta_i}\vec{\rho}\right] \end{aligned}$$

and the off diagonal terms are of the form:

$$\frac{\partial^2 \epsilon}{\partial \theta_i \partial \theta_j} = \frac{2}{n^2}\left[G_i^T G_j\right]$$

so that,

$$\frac{d^2\epsilon}{d\vec{\theta}} = \frac{2}{n}\begin{bmatrix} (\frac{G_1^T G_1}{n} - \frac{\partial G_1^T}{\partial \theta_1}\vec{\rho}) & \frac{G_1^T G_2}{n} & \cdots & \frac{G_1^T G_n}{n} \\ \frac{G_2^T G_1}{n} & (\frac{G_2^T G_2}{n} - \frac{\partial G_2^T}{\partial \theta_2}\vec{\rho}) & \cdots & \frac{G_2^T G_n}{n} \\ & & \vdots & \\ \frac{G_n^T G_1}{n} & \frac{G_n^T G_2}{n} & \cdots & (\frac{G_n^T G_n}{n} - \frac{\partial G_n^T}{\partial \theta_2}\vec{\rho}) \end{bmatrix} \tag{14}$$

$$= \frac{2}{n^2}\begin{bmatrix} G_1^T G_1 & G_1^T G_2 & \cdots & G_1^T G_n \\ G_2^T G_1 & G_2^T G_2 & \cdots & G_2^T G_n \\ & & \vdots & \\ G_n^T G_1 & G_n^T G_2 & \cdots & G_n^T G_n \end{bmatrix} - \frac{2}{n}\begin{bmatrix} \frac{\partial G_1^T}{\partial \theta_1}\vec{\rho} & & & \\ & \frac{\partial G_2^T}{\partial \theta_2}\vec{\rho} & & \\ & & \ddots & \\ & & & \frac{\partial G_n^T}{\partial \theta_2}\vec{\rho} \end{bmatrix} \tag{15}$$

To establish convexity in this metric, we must demonstrate that the eigenvalues of Equation 14 are all positive. Equation 15 demonstrates that this may not be as difficult in general as one might think. The first term in Equation 15 is the product of two matrices, $G^T G$, as is therefore positive (semi)definite. However, as we shall see, care must be taken to guarantee convexity in general.

3.1.2 Force Closure Behavior

The multiplicity of attractors in the control policy illustrated in Figure 2 is addressed by smoothing the image of the object in the wrench domain — or equivalently, smoothing the error surface defined by Equation 10. One "smooth" approximation is the projection of the force domain model of the object onto sinusoidal basis functions with characteristic frequency of $1\frac{cycle}{2\pi\ rad}$.

The force and moment diagrams for this class of objects projected onto the 1^{st} harmonic basis yields:

$$\begin{aligned} w_1 &= f_x = -cos(\theta)cos(\phi) & w_4 &= m_x = 0 \\ w_2 &= f_y = -sin(\theta)cos(\phi) & w_5 &= m_y = 0 \\ w_3 &= f_z = -sin(\phi) & w_6 &= m_z = 0 \end{aligned} \tag{16}$$

Note that using this approximation for n-fold symmetries reduces the control of grasp sufficiency (wrench closure) to a force closure optimization. This is due to the fact that the moment diagrams for n-fold symmetries exhibit characteristic frequencies of $n\frac{cycle}{2\pi}$ and are therefore ignored in the 1^{st} harmonic approximation. Moreover, it can be shown that this wrench model yields a convex sufficiency metric over a portion of the contact configuration space in the planar case when the task wrench bias, $\vec{t} = \vec{0}$ (see Appendix A.2).

The sufficiency metric for this force closure model yields:

$$\begin{aligned} \epsilon_S^{FC} &= \left[\vec{t} - \frac{1}{n}\sum_{i=1}^{n}(\hat{w}_i)\right]^T \left[\vec{t} - \frac{1}{n}\sum_{i=1}^{n}(\hat{w}_i)\right] \\ &= \left[t_{fx} + \frac{1}{n}\sum_{i=1}^{n} cos(\theta_i)cos(\phi_i)\right]^2 + \left[t_{fy} + \frac{1}{n}\sum_{i=1}^{n} sin(\theta_i)cos(\phi_i)\right]^2 + \left[t_{fz} + \frac{1}{n}\sum_{i=1}^{n} sin(\phi_i)\right]^2 \end{aligned} \tag{17}$$

and a contact wrench Jacobian in both the θ and ϕ directions.

$$G_\theta^T = \begin{bmatrix} sin(\theta_1)cos(\phi_1) & -cos(\theta_1)cos(\phi_1) & 0 & 0 & 0 & 0 \\ sin(\theta_2)cos(\phi_2) & -cos(\theta_2)cos(\phi_2) & 0 & 0 & 0 & 0 \\ \vdots & \vdots & & & \vdots & \\ sin(\theta_n)cos(\phi_n) & -cos(\theta_n)cos(\phi_n) & 0 & 0 & 0 & 0 \end{bmatrix} \tag{18}$$

$$G_\phi^T = \begin{bmatrix} cos(\theta_1)sin(\phi_1) & sin(\theta_1)sin(\phi_1) & -cos(\phi_1) & 0 & 0 & 0 \\ cos(\theta_2)sin(\phi_2) & sin(\theta_2)sin(\phi_2) & -cos(\phi_2) & 0 & 0 & 0 \\ \vdots & \vdots & & & \vdots & \\ cos(\theta_n)sin(\phi_n) & sin(\theta_n)sin(\phi_n) & -cos(\phi_n) & 0 & 0 & 0 \end{bmatrix} \tag{19}$$

The gradient of Equation 17 with respect to θ_k yields:

$$\begin{aligned} \frac{\partial \epsilon_S^{FC}}{\partial \theta_k} &= -\frac{2}{n}\left(t_{fx} - \frac{1}{n}\sum_{i\neq k} f_{x,i}\right)\frac{\partial f_{x,k}}{\partial \theta_k} - \frac{2}{n}\left(t_{fy} - \frac{1}{n}\sum_{i\neq k} f_{y,i}\right)\frac{\partial f_{y,k}}{\partial \theta_k} \\ &= \frac{2}{n}\left(t_{fy} + \frac{1}{n}\sum_{i\neq k}(sin(\theta_i)cos(\phi_i))\right)(cos(\theta_k)cos(\phi_k)) - \frac{2}{n}\left(t_{fx} + \frac{1}{n}\sum_{i\neq k}(cos(\theta_i)cos(\phi_i))\right)(sin(\theta_k)cos(\phi_k)) \\ &= A_{\theta k}cos(\theta_k) + B_{\theta k}sin(\theta_k) \\ &= (A_{\theta k}^2 + B_{\theta k}^2)^{1/2}sin(\theta_k + \psi_k) \end{aligned} \tag{20}$$

where,

$$A_{\theta k} = \frac{2}{n}\left(t_{fy} + \frac{1}{n}\sum_{i\neq k}(sin(\theta_i)cos(\phi_i))\right)cos(\phi_k)$$

$$B_{\theta k} = -\frac{2}{n}\left(t_{fx} + \frac{1}{n}\sum_{i\neq k}(cos(\theta_i)cos(\phi_i))\right)cos(\phi_k)$$

$$\psi_k = tan^{-1}(A_{\theta k}/B_{\theta k})$$

This result demonstrates that the sufficiency metric employing the force closure model generates a unimodal error function. Since we want to find the minimum of this error metric, we must satisfy two conditions:

$$(A) \quad \frac{\partial \epsilon_S^{FC}}{\partial \theta_k} \simeq sin(\theta_k + \psi_k) = 0, \ and$$

$$(B) \quad \frac{\partial^2 \epsilon_S^{FC}}{\partial \theta_k^2} \simeq cos(\theta_k + \psi_k) > 0.$$

Condition (A) is the convergence condition and is satisfied at $(\theta_k + \psi_k) = 0,\ \pi$, or

$$\theta_k = -\psi_k,\ \pi - \psi_k.$$

Condition (B) identifies the minimum in the function. The solution to (A) which satisfies this condition is

$$\theta_k^{*} = -tan^{-1}\left(\frac{A_{\theta k}}{B_{\theta k}}\right). \tag{21}$$

Figure 3 illustrates the wrench functions, $f_x(\theta),\ f_y(\theta),\ and\ m_z(\theta)$, the sufficiency metric, and the positions of attractors in the metric space for the smoothed sufficiency metric for the square shape (Figure 2 shows the original wrench model, prior to smoothing). Here, the darkened contact on the right side of the square is fixed in this position. It is clear that since this contact does not respond to the gradient in the sufficiency metric, that we could replace this contact with an equivalent task bias wrench. The resulting sufficiency metric is convex in the interval $[\pi/2, 3\pi/2]$. The controller derived from this metric could be used to optimize the grasp configuration with respect to the sufficiency metric. However, the performance of this controller is sluggish in the vicinity of the maximum and spurious local minima will be introduced if this non-convex control surface is composed with other controllers. Better performance can be achieved by computing a convex (quadratic) controller which has the same stable minima. Appendix B describes a simple quadratic form derived from the smoothed sufficiency error metric. The resulting quadratic can be used to compute the gradient of the convexitized force closure sufficiency metric at contact k.

$$\left.\frac{\partial \epsilon_S}{\partial \theta}\right|_{\theta k}^{FC} = 2\frac{\epsilon_S^{FC} - \epsilon_S^{*}}{(\theta_k - \theta_k^{*})} \tag{22}$$

In practice, stability is enhanced in the vicinity of the equilibrium state if $max(\varepsilon, (\theta_k - \theta_k^{*}))$ is used in the denominator of Equation 22, where ε is a small, positive constant.

Equation 22 was used to generate the solution for a planar grasp on a circular object in Figure 4. In this example, 3 contact locations are controlled by the grasp estimator in a two dimensional force space. The 2D task specification is defined along the $\hat{f}_x$ and $\hat{f}_y$ task basis vectors. The rectangular region plotted in force space depicts a convex set of forces which can be applied by the current contact system. From left to

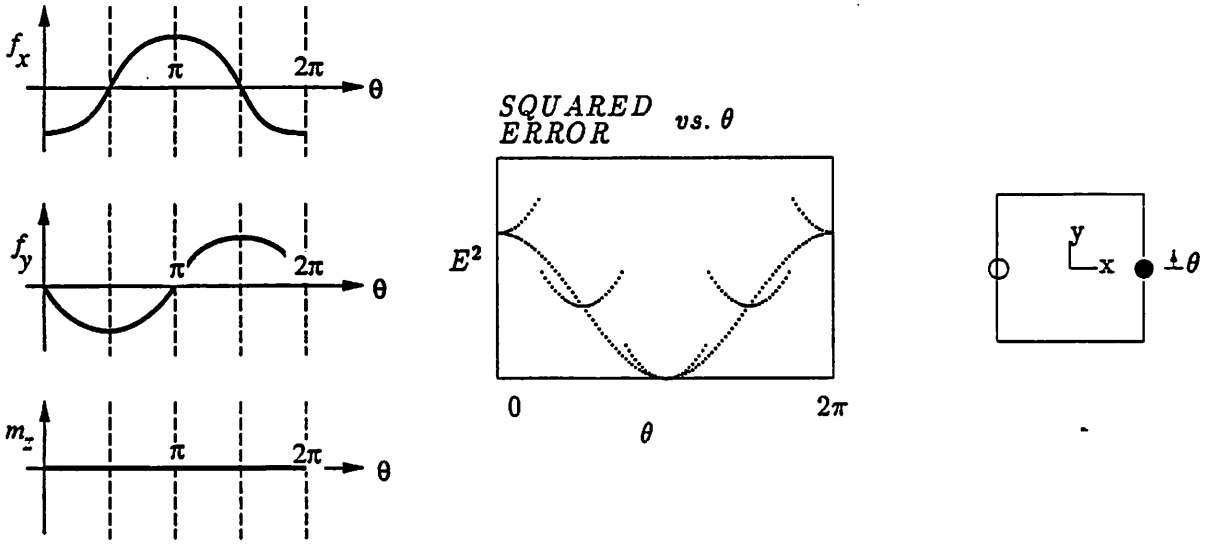

Figure 3: The Approximate Force Model, the Sufficiency Metric ($\vec{t} = \vec{0}$), and the Attractors for the Square. The original error function is superimposed on the smoothed force closure metric.

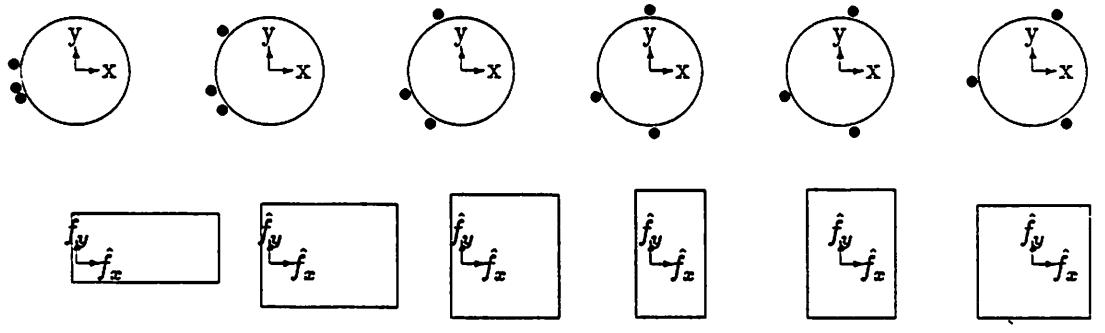

Figure 4: Heuristic Controller for Three Contacts and the Associated Wrench Span of the Contact Configuration

right the contacts migrate from initial to final positions to generate a null space contact geometry — this is an instance of an "optimal" force closure grasp.

A similar quadratic regulator for ϕ_k can be derived by differentiating Equation 17 with respect to ϕ_k,

$$\frac{\partial \epsilon_S^{FC}}{\partial \phi_k} = (A_{\phi k}^2 + B_{\phi k}^2) sin(\phi_k + tan^{-1}(A_{\phi k}/B_{\phi k})) \tag{23}$$

where:

$$\begin{aligned} A_{\phi k} &= \frac{2}{n}\left(t_{mz} + \sum_{i \neq k} sin(\phi_i)\right) \\ B_{\phi k} &= -\frac{2}{n}\left(t_{fx} + t_{fy} + \sum_{i \neq k} cos(\theta_i - \theta_k) cos(\phi_i)\right) \\ \phi_k^{=} &= -tan^{-1}\left(\frac{A_{\phi k}}{B_{\phi k}}\right) \end{aligned}$$

so that,

$$\left.\frac{\partial \epsilon_S}{\partial \phi}\right|_{\phi k}^{FC} = 2\frac{\epsilon_S^{FC} - \epsilon_S^{=}}{(\phi_k - \phi_k^{=})}. \tag{24}$$

3.1.3 Moment Closure Behavior

The approximate wrench models employed in the force closure behavior generate predictable, unimodal control surfaces but disgards a great deal of information in order to do so. The solution generated in this fashion is, therefore, not always expected to be consistent with the minima in the *real* error surface (Figure 2). A local, moment closure optimization can be employed based on enriched force domain information.

Following convergence of the force closure behavior, contacts are positioned on particular planar facets of the object. The moment closure optimization will adjust the contact placement to eliminate any residual moment in the grasp. We use the perpendicular of a plane, (r_0, θ_0, ϕ_0), to parameterize the contact plane. Figure 5 illustrates the parameterization and the geometry from which the wrench models are derived. The forces transmitted through any planar face are constant at all contact positions on that face. The moments applied to the object, $\vec{m} = \vec{r} \times \vec{f}$, vary linearly with surface coordinate and pass through zero where the perpendicular passes through the plane. The resulting wrench model is:

$$\begin{aligned} w_1 &= f_x = -cos(\theta_0)cos(\phi_0) & \qquad w_4 &= m_x = -r_\theta sin(\phi_0)cos(\theta_0) + r_\phi sin(\theta_0) \\ w_2 &= f_y = -sin(\theta_0)cos(\phi_0) & \qquad w_5 &= m_y = -r_\theta sin(\phi_0)sin(\theta_0) - r_\phi cos(\theta_0) \\ w_3 &= f_z = -sin(\phi_0) & \qquad w_6 &= m_z = r_\theta cos(\phi_0) \end{aligned} \tag{25}$$

where (r_θ, r_ϕ) are the surface coordinates of the contact in the plane. Note that this local planar surface approximation yields constant contact forces which implies that control is derived from the moment diagrams exclusively.

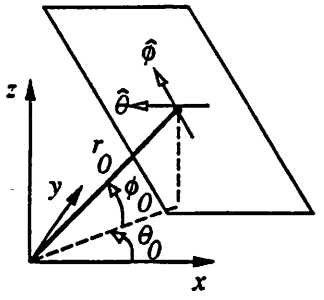

$$\hat{\phi}^T = [\, -sin(\phi_0)cos(\theta_0),\ -sin(\phi_0)sin(\theta_0),\ cos(\phi_0)\,]$$
$$\hat{\theta}^T = [\, -sin(\theta_0),\ cos(\theta_0),\ 0\,]$$
$$\hat{f}^T = [\, -cos(\theta_0)cos(\phi_0),\ -sin(\theta_0)cos(\phi_0),\ -sin(\phi_0)\,]$$

Figure 5: The Moment Closure Model derived from a Parametric Object Plane

The moment closure sufficiency metric can be written as follows.

$$\begin{aligned}
\epsilon_S^{MC} &= \left[t_{fx} - \frac{1}{n}\sum_i(-cos(\theta_0)cos(\phi_0))\right]^2 + \left[t_{fy} - \frac{1}{n}\sum_i(-sin(\theta_0)cos(\phi_0))\right]^2 + \left[t_{fz} - \frac{1}{n}\sum_i(-sin(\phi_0))\right]^2 \\
&+ \left[t_{mx} - \frac{1}{n}\sum_i(-r_\theta sin(\phi_0)cos(\theta_0) + r_\phi sin(\theta_0))\right]^2 + \left[t_{my} - \frac{1}{n}\sum_i(-r_\theta sin(\phi_0)sin(\theta_0) - r_\phi cos(\theta_0))\right]^2 \\
&+ \left[t_{mz} - \frac{1}{n}\sum_i(r_\theta cos(\phi_0))\right]^2 \qquad (26)
\end{aligned}$$

For this model, the contact wrench Jacobian for surface coordinate, r_θ is:

$$G_{r\theta}^T = [0, 0, 0, -sin(\phi_0)cos(\theta_0), -sin(\phi_0)sin(\theta_0), cos(\phi_0)]$$

and,

$$\frac{\partial G_{r\theta}^T}{\partial r\theta} = \vec{0}.$$

This result immediately establishes global convexity for the moment closure sufficiency metric by noting that the second term in Equation 15 is zero and the resulting Hessian is just G^TG. The product of any matrix with itself is trivially positive definite and symmetric.

The controller is derived from this convex surface by transforming from planar surface coordinates to polar coordinates and then constructing a quadratic regulator with the same equilibrium state as the original convex metric. Note that $\partial G_\theta^T/\partial\theta$ is not generally convex, but that $\partial G_{r\theta}^T/\partial r\theta$ is, as was demonstrated above. The planar surface coordinate where the gradient of ϵ_S^{MC} with respect to r_θ vanishes at

$$\begin{aligned}
\bar{r_{\theta k}} &= -\left[nt_{mx} + \sum_{i\neq k}(r_\theta sin(\phi_0)cos(\theta_0) - r_\phi sin(\theta_0))\right](sin(\phi_0)cos(\theta_0))_k \\
&- \left[nt_{my} + \sum_{i\neq k}(r_\theta sin(\phi_0)sin(\theta_0) + r_\phi cos(\theta_0))\right](sin(\phi_0)sin(\theta_0))_k \\
&+ \left[nt_{mz} - \sum_{i\neq k}(r_\theta cos(\phi_0))\right](cos(\phi_0))_k
\end{aligned}$$

This extremum is a global minimum since the metric is convex (positive definite). The corresponding θ coordinate of this minimum is:

$$\theta_k^{=} = tan^{-1}\left[\frac{r_{\theta k}^{=}}{r_0}\right] \tag{27}$$

so that,

$$\left.\frac{\partial \epsilon_S}{\partial \theta}\right|_{\theta k}^{MC} = 2\frac{\epsilon_S^{MC} - \epsilon_S^{=}}{(\theta_k - \theta_k^{=})}. \tag{28}$$

A similar result for the moment closure regulator in the $\hat{\phi}$ direction can be derived by differentiating Equation 25 with respect to ϕ_k.

$$G_{r_{\phi},k}^T = [0, 0, 0, -sin(\theta_0), cos(\theta_0), 0] \tag{29}$$

and, as before, $\partial G^T / \partial r_\phi = \vec{0}$ establishes the fact that the sufficiency metric for the moment closure model is globally convex. If we differentiate Equation 26 with respect to ϕ_k, and setting the result to zero, we can solve for the surface coordinate, $r_\phi^{=}$, that minimizes the moment closure sufficiency metric.

$$\begin{aligned} r_{\phi k}^{=} \;=\; & -\left[nt_{mx} + \sum_{i \neq k}(r_\theta sin(\phi_0)cos(\theta_0) - r_\phi sin(\theta_0))\right](sin(\theta_0))_k \\ & -\left[nt_{my} + \sum_{i \neq k}(r_\theta sin(\phi_0)sin(\theta_0) + r_\phi cos(\theta_0))\right](cos(\theta_0))_k \end{aligned}$$

This extremum is a global minimum since the metric is convex (positive definite). The corresponding ϕ coordinate of this minimum is:

$$\phi_k^{=} = tan^{-1}\left[\frac{r_{\phi k}^{=}}{r_0}\right] \tag{30}$$

so that,

$$\left.\frac{\partial \epsilon_S}{\partial \phi}\right|_{\phi k}^{MC} = 2\frac{\epsilon_S^{MC} - \epsilon_S^{=}}{(\phi_k - \phi_k^{=})}. \tag{31}$$

3.1.4 Wrench Closure Composition

The goal of this behavior composition is to construct a null space in the contact wrench space of the object. The problem is formulated as an optimization of the sufficiency metric. However, we have demonstrated that this metric will have local minima which do not yield sufficient grasp configurations. This problem is addressed by employing two distinct control surfaces. The first regulates the contact configuration using a heuristic, force closure model of the object consisting of the projection of the wrench space image of the object onto a sinusoidal basis function with characteristic frequency $1 cycle/2\pi$. The second employs a moment closure model consisting of locally planar object geometry mapped into the force domain.

This set of behaviors is capable of producing "correct" grasps in the sense of Principle 3.1 for n-fold, convex, rotational symmetric objects. This follows from the observation that if the force closure regulator is permitted to run until convergence, then the moment closure behavior does not need to leave the current object face to eliminate any residual moment.

It is our hope that we may actually use these behaviors as the basis for a more general grasp controller. To that end, we propose to activate wrench closure behaviors in a context dependent manner. The work described here has counterparts in earlier robotics research. The behaviors described earlier for grasping have been activated in a finite state automaton[19] — this work was patterned after similar work on hopping platforms[38]. It was demonstrated that such machines could be used to generate "gaits" in system behavior representing manipulation sequences. More recent work has viewed the composition problem in the context of the system utility of competing controllers.

This work employs a form of radial basis function to activate a set of competitive behaviors on the basis of the system state. Luce's rule is a composition function derived from game theory which permits the introduction of multiple decision surfaces, the shaping/profiling of the decision hyperplane, and which admits domain knowledge in the form of *a priori* structure for competing behaviors. Luce's rule is used to express (hyper)planar decision surfaces in error space and to shape the activation in the neighborhood of a decision using an exponential switching profile.

$$A_i = \frac{e^{\gamma_i}}{\sum_j e^{\gamma_j}} \tag{32}$$

where:

$$\begin{aligned} A_i &= \text{activation coefficient of behavior } i\text{,such that } \sum_i A_i = 1. \\ \gamma_i &= \text{the weighted error metric associated with behavior } i. \end{aligned} \tag{33}$$

The switching boundary is modulated by specifying three parameters (r, θ, σ)

r — the length of the perpendicular *constructor* of the switching boundary;

θ — the orientation of the perpendicular constructor;

σ — the steepness of the switching profile, expressed as the gradient magnitude at the switching boundary.

Combinations of these parameters can be used to adjust the position, orientation, and switch profile of the decision surface.

We will use a particularly simple composition strategy consisting of a single linear decision surface to distinguish two linearly separable activation domains in the error space — or equivalently a single radially symmetric activation function in the state space. This is a relatively inexpressive composition rule, but is sufficient for this class of objects. The decision surface is a relatively sharp profile with parameters $r = 0.01$, $\theta = 0.0$, $\sigma = 500.0$ so that the activation of the wrench closure behaviors is:

$$A_{FC} = \frac{e^{(\gamma_{FC} - \gamma_{MC})}}{(1 + e^{(\gamma_{FC} - \gamma_{MC})})} \tag{34}$$

$$A_{MC} = 1 - A_{FC} \tag{35}$$

The corresponding decision boundary for this activation function is shown in Figure 6. We arrived at these values by experimenting within a range of values for each parameter over a set of 10 objects, as detailed in the next section. Overall worst-case and average scores were computed, and the parameters above represent the best choices, according to our metric.

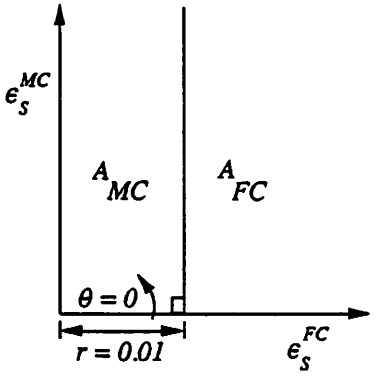

Figure 6: The Decision Surface Separating Force Closure and Moment Closure Activation

If $d\epsilon_S^{FC}/d\vec{\psi}_k$ and $d\epsilon_S^{MC}/d\vec{\psi}_k$ are the gradients for force closure and moment closure respectively, where $\vec{\psi}_k = (\theta, \phi)_k$ is the coordinate of contact k, then the composite gradient is:

$$\frac{d\epsilon_S}{d\vec{\psi}_k} = A_{FC}\frac{d\epsilon_S^{FC}}{d\vec{\psi}_k} + A_{MC}\frac{d\epsilon_S^{MC}}{d\vec{\psi}_k}. \tag{36}$$

The controller employed to regulate wrench closure is derived from the composite gradient.

$$\Delta\vec{\psi}_k = -K_{WC}\frac{d\epsilon_S}{d\vec{\psi}_k} \tag{37}$$

Wrench Closure Performance

Figure 7 is a plot of the behavior activation profile for one of two fingers during grasp formation on the square shape. These results are qualitatively the same as for all numbers of contacts and over all shapes that we evaluated. The initial activation for this grasp (see Figure 7(a)) is entirely force closure. During this phase of the grasp, the wrench closure composition by passes a local minimum in the moment closure sufficiency metric (Figures 7 (b) and (c)).

One may view the grasp synthesis process as one which initially employs the force closure behavior to select a set of contact faces, and which subsequently refines the solution using the moment closure behavior (a more precise model of the real wrench surface). Regardless of the particular set of contact surfaces selected, the moment closure behavior can always succeed in eliminating any residual moment in the grasp for the objects we tested. This grasp synthesis process is correctly viewed as a force closure heuristic directing a "best only" search which is subsequently optimized locally. The proposed composition of convex controllers generates a number of distinct solutions. In fact, the value of the equilibrium error can be used to identify topologically distinct solutions, each of which can be realized in an infinite number of geometric solutions.

The performance of the system was evaluated on the planar shapes illustrated in Figure 8. Figure 9 illustrates all the distinct grasps that were generated by the controller for the test shapes. The grasp estimator was executed 100 times for each of 2, 3, and 4 contacts for each shape. Figure 10 shows the distribution of run-time required for convergence of the grasping behaviors for this sample. Figure 10 reports the mean number of single control steps until convergence from random initial configurations. A

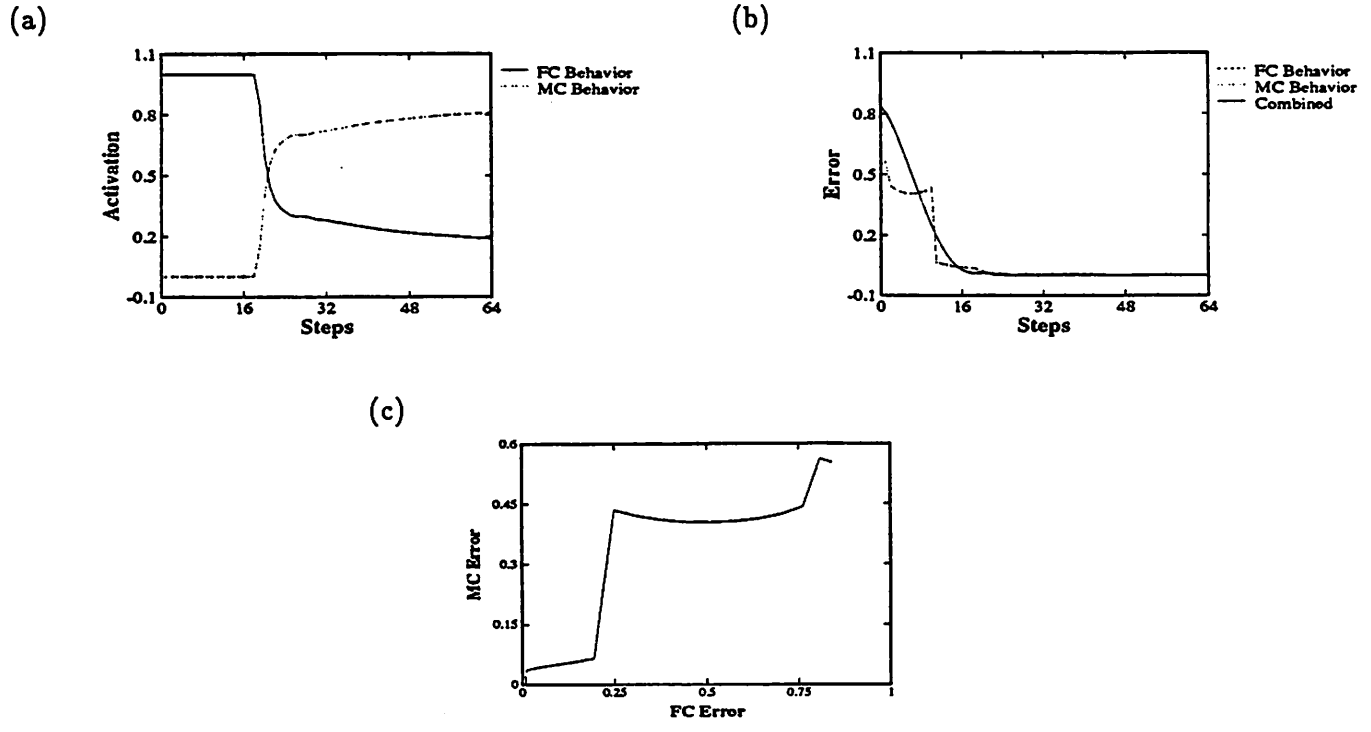

Figure 7: Wrench closure control dynamics for the formation of a grasp: (a) activation profile, (b) force and moment closure sufficiency error, and (c) the resulting trajectory in the wrench closure error plane.

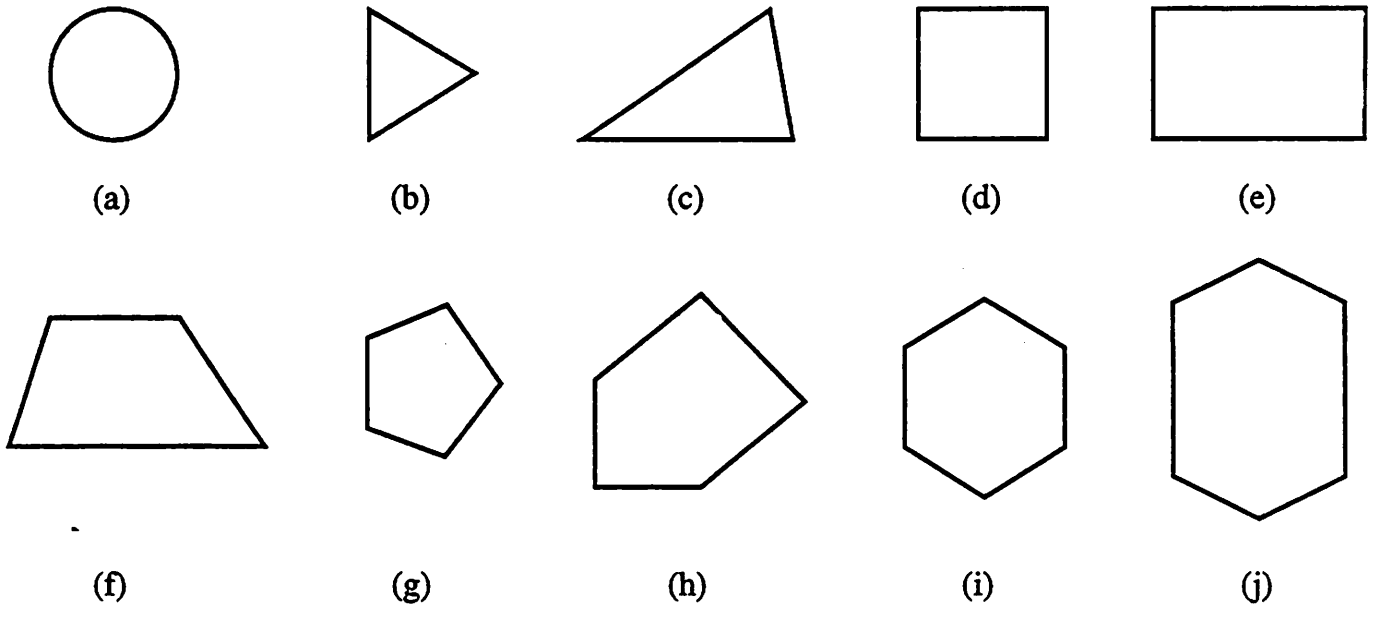

Figure 8: Objects used in the experiments: (a) circle, (b) regular triangle, (c) irregular triangle, (d) square, (e) rectangle, (f) trapezoid, (g) regular pentagon, (h) irregular pentagon, (i) regular hexagon and (j) irregular hexagon

single step in the controller is one adjustment of the contact configuration. That is, a single adjustment of all n contacts. The algorithm is $O(n^2)$ each step, where n is the number of contacts. For a 4 contact grasp estimator, this corresponds to 1.8 milliseconds of CPU time per step on SPARCstation 2 workstation. This complexity can be reduced for large n by running n-$O(n)$ controllers — one for each contact position.

3.2 Managing Mechanical Redundancy

3.2.1 The Manipulability Index

The *manipulability ellipsoid* is used in this work to characterize a manipulator's ability to generate forces and velocities[48]. The Principal Kinematic Axes (PKAs) of each finger may be identified by examining the transformation from joint space to Cartesian space expressed by the Jacobian. The singular value decomposition is employed to represent the character of the transformation. For a complete and detailed description of the singular value decomposition see Golub *et al.* [17].

If we map the unit sphere in R^4

$$\|\dot{\theta}\| = \dot{\theta}_1^2 + \dot{\theta}_2^2 + \dot{\theta}_3^2 + \dot{\theta}_4^2 \tag{38}$$

into Cartesian R^3 space through the Jacobian, the result is the manipulability ellipsoid proposed by Yoshikawa[47]. The ellipsoid describes the Cartesian character of the *amplification* in the Jacobian transform from joint velocities to Cartesian velocities. If the singular value decomposition of the Jacobian is

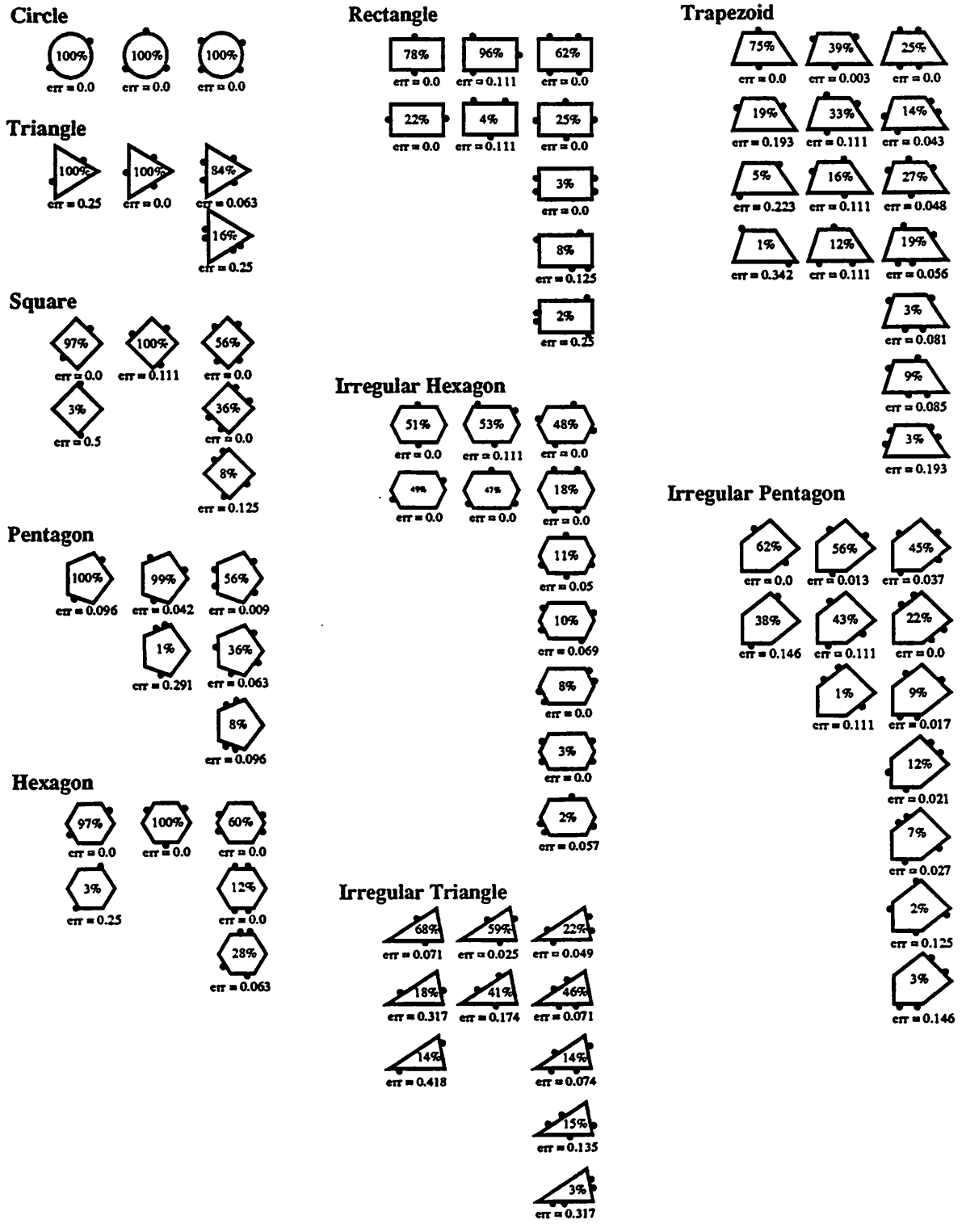

Figure 9: The grasp types for all objects tested. Percentages reported represent the fraction of random initial contact configurations that led to each solution type. Also recorded is the residual wrench closure error at convergence.

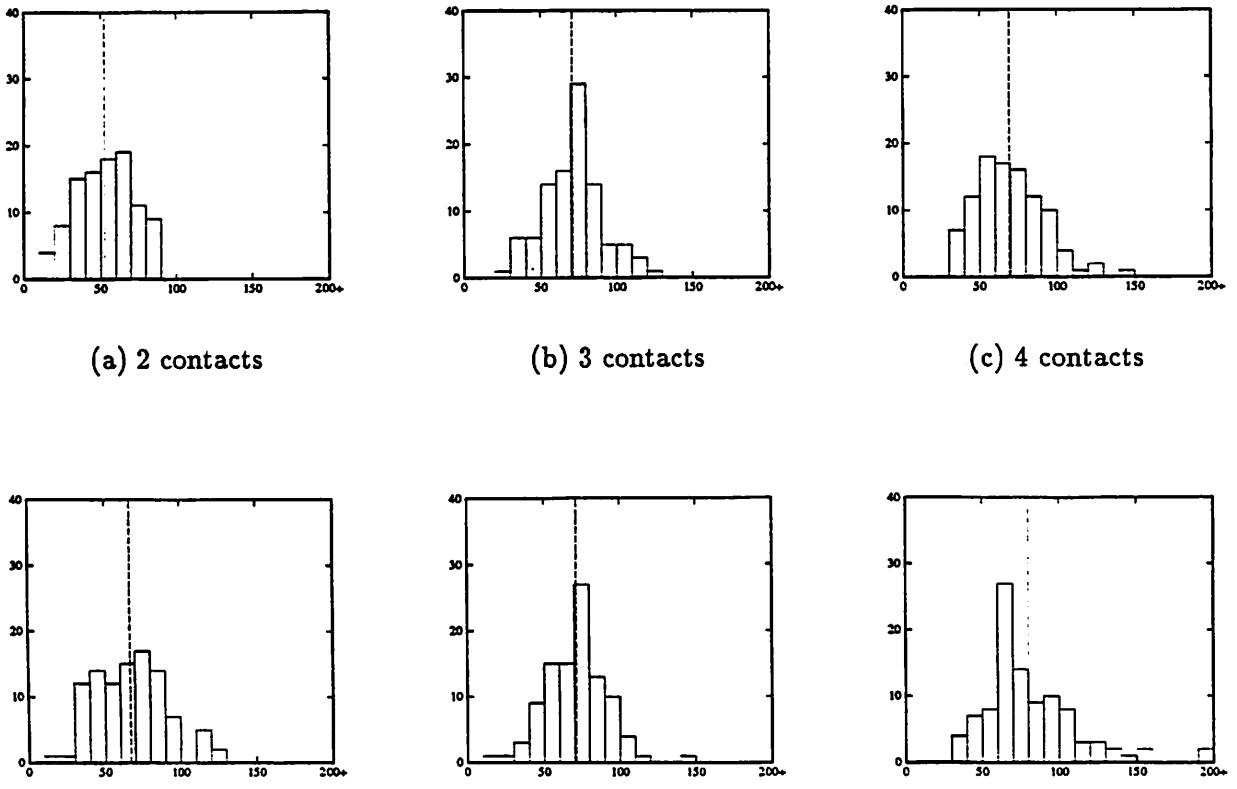

(a) 2 contacts (b) 3 contacts (c) 4 contacts

(d) 2 contacts (e) 3 contacts (f) 4 contacts

Figure 10: Histogram of number of steps until convergence for 2, 3, and 4 contacts. The top row illustrates the results for the pentagon, the bottom row represents the irregular pentagon.

Object	Number of contacts	Average # Steps	Standard Deviation
Circle	2	39.450000	10.779118
	3	59.020000	14.169237
	4	60.070000	16.905115
Triangle	2	58.740000	15.180144
	3	124.780000	62.848637
	4	67.650000	23.916680
Square	2	60.460000	20.197720
	3	69.610000	19.215364
	4	71.250000	20.847874
Pentagon	2	52.370000	18.321294
	3	70.860000	20.051963
	4	69.190000	21.734716
Hexagon	2	56.970000	18.359736
	3	88.880000	28.329690
	4	69.230000	15.542613
Rectangle	2	62.500000	19.279182
	3	76.960000	28.193387
	4	74.120000	20.630604
Irregular Hexagon	2	57.480000	20.915163
	3	69.180000	22.986768
	4	67.000000	19.614466
Irregular Triangle	2	73.910000	35.863404
	3	94.080000	41.885771
	4	86.150000	39.127705
Trapezoid	2	78.910000	45.363202
	3	89.720000	36.505729
	4	70.610000	30.680463
Irregular Pentagon	2	66.590000	23.036684
	3	71.230000	19.774412
	4	80.240000	31.220338

Table 1: Numbers of steps until convergence, averaged over 100 trials.

computed, the manipulability ellipsoid is described by the Principal Kinematic Axes (PKAs):

$$\{\sigma_1\vec{u_1}, \sigma_2\vec{u_2}, \sigma_3\vec{u_3}\} \tag{39}$$

where the σ_i are the singular values and the $\vec{u_i}$ are the corresponding singular vectors.

Chiu[10] points out that the singular vectors for the force relationship $\vec{\tau} = J^T\vec{f}$ are the same as those describing the velocity domain, but that the singular values are reciprocal. This suggests that the direction for favorable velocity amplification is orthogonal to the direction for favorable force amplification. Moreover, since accuracy is inversely proportional to amplification, a reciprocal relationship also exists between accuracy and amplification in both the velocity and force domains.

The manipulability index of the finger is a scalar metric describing the conditioning of the kinematic transformation [48]. The index is proportional to the ellipsoidal volume spanned by the PKAs. This volume is approximated in practice by the product of the singular values. Since the volume of an ellipse increases as the ellipse becomes more spherical, there is a correlation between high manipulability indices and isotropic conditioning.

3.2.2 Manipulability-Based Spatial Isotropy

Figure 11 illustrates the manipulability index computed over the workspace of the Utah/MIT finger. This model is computed within the medial plane of the finger, ie. for $\theta_0 = 0$.

The manipulability models are computed by enumerating all joint configurations for the finger and saving those configurations which produce the largest index at each Cartesian location in a regular sampling of the workspace. The sampling in this case was on a rectangular, 0.002 meter grid.

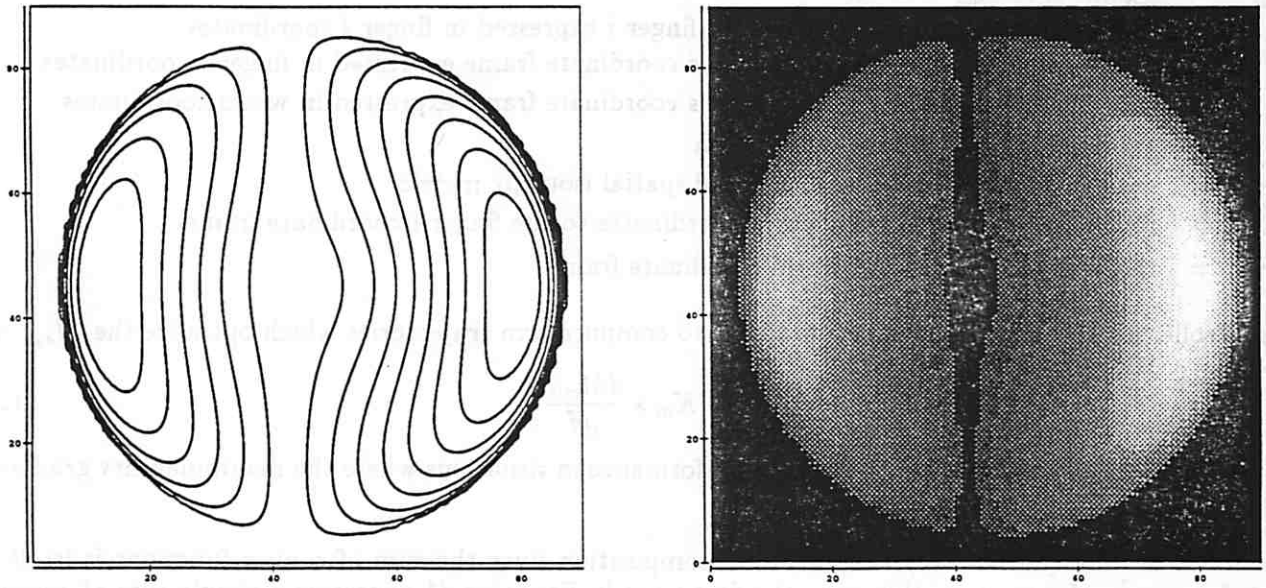

Figure 11: The Max-Manipulability Model for the Utah/MIT Finger/Thumb

The controller that regulates the arm posture ascends the system manipulability metric. The system manipulability is a convex composition of independent, convex fields (note: only a portion of the manipulability

field is convex for the Utah/MIT finger kinematics, even less for the thumb).

$$M_{sys} = \sum_i m_i$$

If the contact geometry is held fixed, then the posture of the hand/arm system can be optimized by gradient ascent with respect to posture modifications.

The gradient is computed as follows:

$$\frac{\partial M_{sys}}{\partial \vec{\theta}}^T = \left[\frac{\partial M_{sys}}{\partial \theta_0}, \frac{\partial M_{sys}}{\partial \theta_1}, \frac{\partial M_{sys}}{\partial \theta_2}, \frac{\partial M_{sys}}{\partial \theta_3}\right] \tag{40}$$

Notice that θ_i in the above expression refers to the arm's joint angles. The objective here is to maximize the system manipulability. in general purpose manipulation devices. This permits the system to react to unexpected interaction with the environment, and can be used to reflexively adjust the hand/arm posture in response to a task level command.

The gradient can be computed as follows:

$$\frac{dM_{sys}}{d\vec{\theta}} = \sum_i \underbrace{\frac{\partial M_{sys}}{\partial m_i}\frac{\partial m_i}{\partial \vec{x}_i}}_{\text{convex scalar field}} \; {}_{f_i}R_w \; \underbrace{\frac{\partial \vec{X}_i}{\partial \theta}}_{\text{arm Jacobian}} \tag{41}$$

where:

M_{sys}	=	$\sum_i m_i \implies \frac{\partial M_{sys}}{\partial m_i} = 1.$
m_i	=	the scalar manipulability metric for finger i expressed in finger i coordinates
$\vec{x}_i$	=	the position of the origin of finger i's coordinate frame expressed in finger i coordinates
$\vec{X}_i$	=	the position of the origin of finger i's coordinate frame expressed in world coordinates
$\frac{\partial M_{sys}}{\partial m_i}$	=	gradient of the composition function
$\frac{\partial m_i}{\partial \vec{x}_i}$	=	gradient of the manipulability-based spatial isotropy metric
${}_{f_i}R_w$	=	rotational transform from world coordinates to the finger i coordinate frame
$\frac{\partial \vec{X}_i}{\partial \theta}$	=	the arm Jacobian in the world coordinate frame

The controller utilizes this performance gradient to compute arm trajectories which optimize the M_{sys} of the task:

$$\Delta\vec{\theta} = K_m * \frac{dM_{sys}}{d\vec{\theta}} \tag{42}$$

In practice, K_m is normalized gain to improve performance in situations where the manipulability gradient gets shallow.

The summation in Equation 41 yields a convex composition since the sum of convex functions is itself a convex function[2]. Moreover, in this case, the first term in Equation 41 expresses a simple sum of convex performance indices associated with each finger, and is therefore a convex composition as well. The second term, $\frac{\partial m_i}{\partial \vec{x}_i}$, is the gradient of a convex scalar field describing "manipulability" (illustrated in Figure 11). However, Equation 41 in its entirety is not in general convex because of the manipulator Jacobian. We

[2]positive definite Hessians sum to positive definite Hessians

cannot hope to do better than this since this non-convexity expresses the character of the particular manipulator employed to move the hand about in the world. Reflexive controllers cannot be expected to provide the deliberative behavior required to optimally posture the arm for the task, they are appropriately used to react to haptic information to generate small refinements to a predetermined nominal strategy.

Figure 12 illustrates the fingertip trajectories resulting from arm adjustments based on the manipulability gradient. The arm configuration for this example was the initial configuration illustrated in Figure 13. Figure 13 illustrates the behavior of this reflexive arm configuration controller when all four fingers influ-

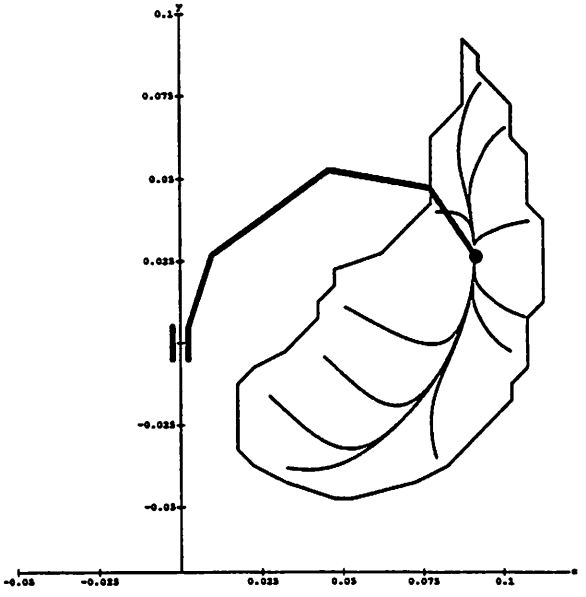

Figure 12: The Relative Fingertip Trajectories Resulting from the Manipulability Reflex

ence the arm posture. This example is the trace of the controller (Equation 41) executed on the hand/arm system[3]. Suppose the hand expected to encounter a plane parallel to the $y - z$ plane while moving i the x direction. Instead, suppose that it encounters a plane that is inclined 45°. The dotted hand/arm configuration in Figure 13 represents the hand configuration resulting from this encounter with the inclined planar surface. The solid hand/arm shows the result of the reflexive, manipulability-based posture correction.

All four fingers have been reconfigured simultaneously during this reposturing. The hand is again compliant to unexpected interactions with the environment, or to strategic contact placement. This is a direct consequence of employing the manipulability as our performance metric — which seeks isotropic hand states.

A vertical (model) plane was expected and a hand trajectory normal to this hypothetical plane was selected initially. From the perspective of the hand, the new posture has transformed the observed plane into the model plane. The hand plane relationship is now approximately equivalent to that expected during the planning stages of this motion. The model of the world has been reflexively transformed into registration with observation.

[3]The hand/arm system consists of a Utah/MIT hand and a GE P50 robot arm.

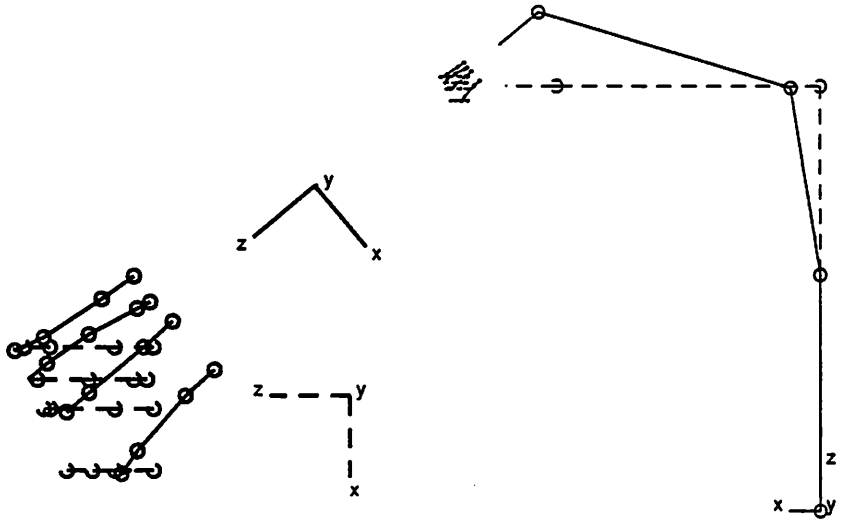

Figure 13: Reflexive Adjustment of Arm Posture to Optimize Hand Manipulability. The dotted lines define the initial hand/arm configuration, the final configuration is drawn with solid lines. Fingertip positions remain constant.

4 Hand/Arm Grasp Control

Table 2 is a synopsis of the independent controllers for achieving aspects of wrench closure developed in the preceeding sections.

Figure 14 illustrates a structure for the dynamic recomposition of a grasp controller. The elemental controllers are the leaves of a control tree structure for each kinematic chain in the robot. The structure of each tree is derived from the assumptions employed during behavior design. For instance, the moment closure behavior competes with the force closure behavior without considering the manipulator posture. The consensus wrench closure composition then runs concurrently with the manipulability-based posture controller. Figure 15 illustrates the behavior of this reflexive arm configuration controller in a two-fingered grasp situation.

5 Conclusion

We have demonstrated the performance of a hand/arm controller which is designed to generate multifingered, dextrous grasps on rotationally symmetric, convex shapes. The results support the value of this approach for improving the run-time performance of controllers for high dimensional systems. We have also experimented with the ability of such a local grasp estimator to reject bounded uncertainty in a grasp plan. To test this idea, the proposed controller was examined while it performed grasp estimates from random initial configurations, rather than from planned contact configurations. The result for this class of objects suggests that even a rather brute-force behavioral composition produced robust results despite the fact that the estimator revised the grasp estimate from arbitrarily bad initial configurations. The grasp estimator could, in fact, alleviate the need for planning grasps at all for this class of objects. It exhibits a great deal of local competency is this type of grasping task and under these circumstances it is capable of

WRENCH CLOSURE BEHAVIOR	CONTROLLER
force closure	$\frac{\partial \epsilon_S}{\partial \theta}\Big\|_{\theta k}^{FC}$ = Equation 22 $\frac{\partial \epsilon_S}{\partial \phi}\Big\|_{\phi k}^{FC}$ = Equation 24
moment closure	$\frac{\partial \epsilon_S}{\partial \theta}\Big\|_{\theta k}^{MC}$ = Equation 28 $\frac{\partial \epsilon_S}{\partial \phi}\Big\|_{\phi k}^{MC}$ = Equation 28
composition	A_{FC} = Equation 34 A_{MC} = Equation 35
SPATIAL ISOTROPY BEHAVIOR	CONTROLLER
manipulability	Equation 42

Table 2: Constituent Hand/Arm Controllers for Grasp Formation

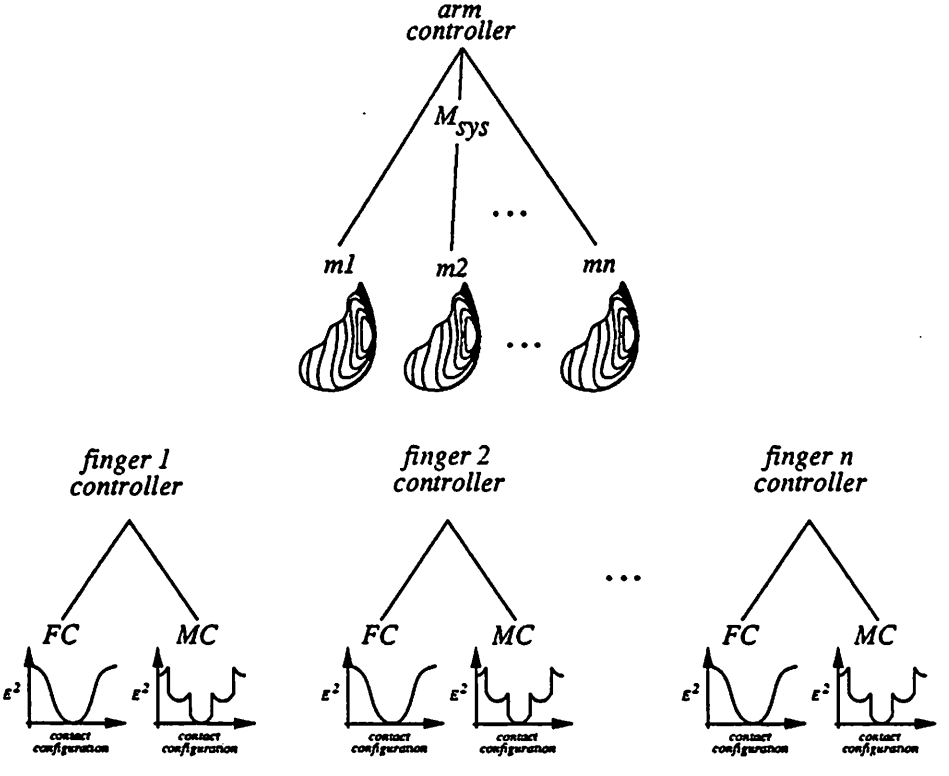

Figure 14: Asynchronous, Reactive Grasp Controllers

model-less grasping. It is probably also true that the same approach can suppress uncertainty during the execution of a knowledge-based grasp for more general object shapes. We have also devised a means for extracting object models from vision and proprioceptive information in the hand. This sensory apparatus permits an object model to be constructed incrementally during grasp formation. It is possible that the same model can provide a reactive context for reflexive behavior composition. We view this currently, as a reinforcement learning problem where knowledge about object geometry influences the composition of reflexive grasp estimators. The choice of the behaviors presented in this paper was heavily influenced by a commitment to incremental, sensor-based reactive controllers and to the learning problem.

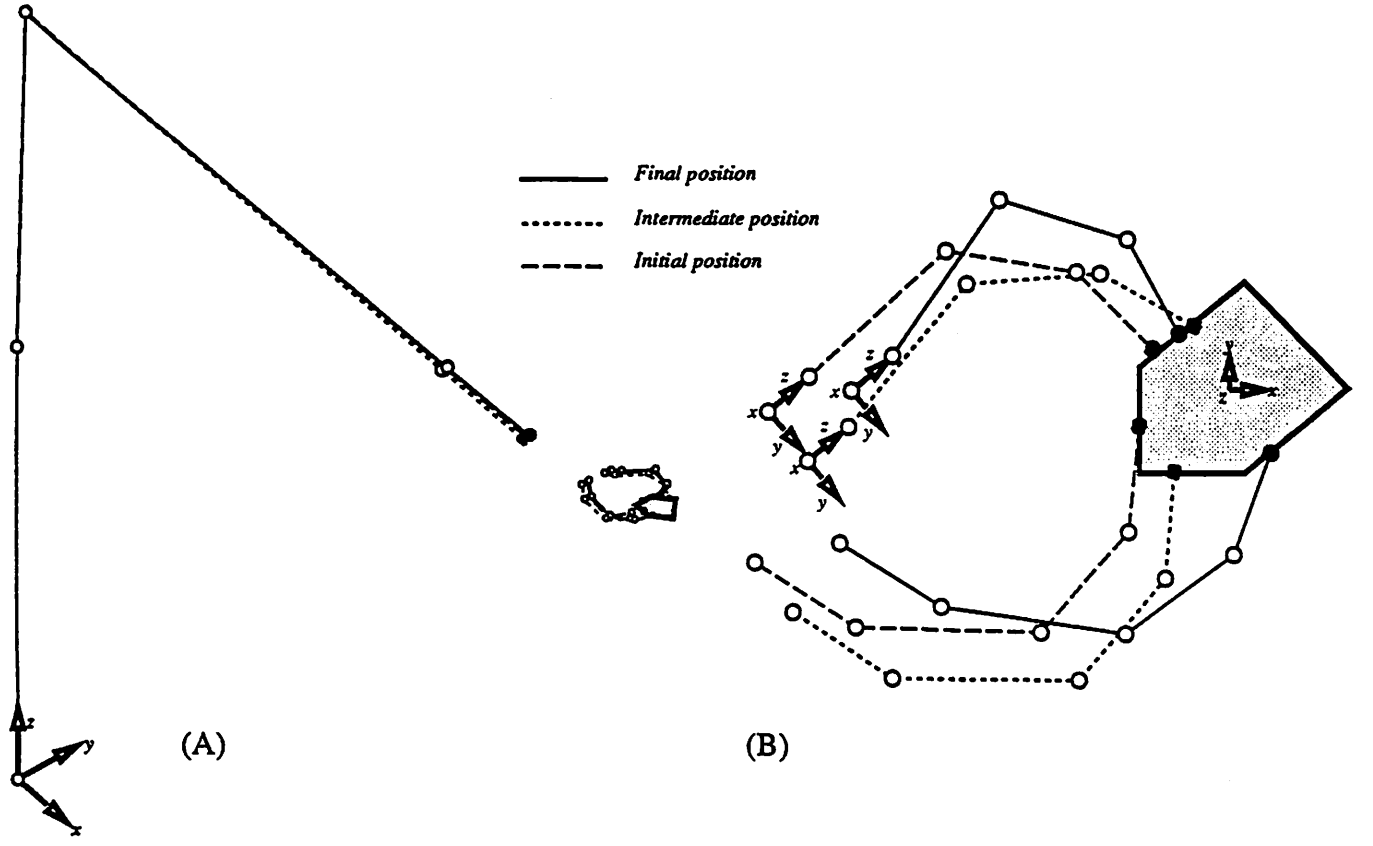

(C)

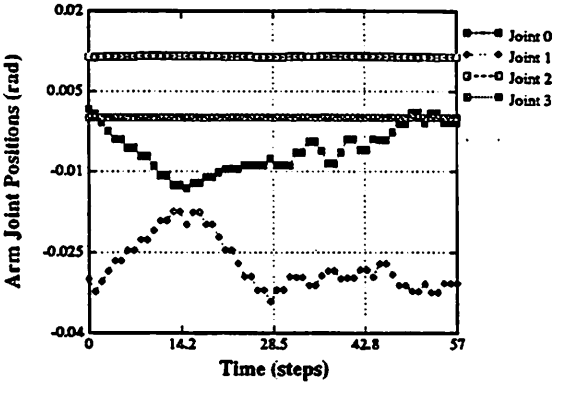

Figure 15: Behavioral Repertoire Applied to the Irregular Pentagon. (A) The hand-arm-object solution, (B) a detail of the grasp solution, and (C) the arm angles during grasp formation.

A Admissible Controllers

Another long term goal of this work is to discover properties by which high dimensional state spaces may be decomposed into computationally tractable subspaces. The on-line recomposition of behavior must certainly consider the complex interactions that exist between behavioral sub-spaces. This suggests that the composition of behavior will itself be a dynamic process. It is necessary to constrain the expression of elemental behaviors so that this dynamic composition process yields admissible composite control surfaces.

Rimon and Koditschek[46] established a formal basis with which to define a class of admissible *navigation* functions. The work addresses the "find-control-law" problem in configuration space which maps the robot state — position and velocity — into torque inputs at each joint which results in a feedback compensator that moves to the goal without hitting obstacles. The planning phase does not generate a sequence of reference positions for the robot controller, but instead designs the controller itself. Rimon *et.al.* define a suitable navigation function as one which;

1. is analytic on the domain — continuously differentiable and expressible as a power series at every point,
2. is polar — there is a unique position within the domain of any behavior where the gradient of the scalar metric field goes to zero.
3. is Morse on the domain — non-singular Hessian implies no "stacked-up" saddle points,
4. has its maximal value uniformly/exactly on the boundary, and
5. bounded gradient magnitude — there is a compact neighborhood about the single extremum where the gradient magnitude is less than ϵ. This implies that controllers derived from the scalar field can be guaranteed to converge to within this neighborhood.

These properties are important characteristics of control surfaces that guarantee that predictable controllers may be derived from local properties of the control (or navigation) function.

Connolly and Grupen[11, 22] show applications of harmonic functions in robot control motivated by similar formal properties of admissible control functions. Connolly *et.al.* illustrate a means of deriving controllers from harmonic solutions over the robot's configuration space. Any motion constraint that projects onto the configuration space may be used in theory to incrementally modify the control surface employed by the robot. Both Rimon *et.al.* and Connolly *et.al.* attempt to provide a formalized basis for control subject to constraints expressed in the configuration space. In the Rimon *et.al.* approach which relies on conformal deformations of spherical geometries, environmental complexity and system dimensionality are challenging practical issues. In the Connolly *et.al.* work, it is theoretically possible that individual configuration spaces may be cascaded to yield higher dimensionality, but this approach has not yet been demonstrated.

A.1 Properties of the Hessian

If given a multivariable control function, F, defined on domain, Θ, we may classify the admissibility of F into several categories based on properties of the Hessian of F, $\partial^2 F/\partial\Theta^2$.

$$\partial^2 F/\partial\Theta^2 = \begin{bmatrix} \frac{\partial^2 F}{\partial\theta_1^2} & \frac{\partial^2 F}{\partial\theta_1\partial\theta_2} & \cdots & \frac{\partial^2 F}{\partial\theta_1\partial\theta_n} \\ & \vdots & \vdots & \\ \frac{\partial^2 F}{\partial\theta_n\partial\theta_1} & \frac{\partial^2 F}{\partial\theta_n\partial\theta_2} & \cdots & \frac{\partial^2 F}{\partial\theta_n^2} \end{bmatrix} \tag{43}$$

Convex Control Functions: If the Hessian is positive (semi-)definite over the domain Θ, then the function F is convex over Θ. Intuitively, this is equivalent to requiring the change in slope of the tangent to the control surface to be monotonic along any section through the surface. Such a control surface will possess a single extremum (minimum for positive definite) and if that extremum is in the interior of Θ, then the control surface will converge to this point.

A necessary and sufficient condition for positive definite-ness of the Hessian is presented in Theorem A.1.

Theorem A.1 (Sylvester) *$H \in R^n \times R^n$ is positive definite iff the following n determinants are all positive:*

$$\begin{aligned} D_1 &= H_{11} > 0 \\ D_2 &= \begin{vmatrix} H_{11} & H_{12} \\ H_{21} & H_{22} \end{vmatrix} > 0 \\ &\vdots \\ D_n &= \begin{vmatrix} H_{11} & H_{12} & \cdots & H_{1n} \\ & \cdot & & \\ H_{n1} & H_{n2} & \cdots & H_{nn} \end{vmatrix} > 0 \end{aligned}$$

The converse of this theorem is not true; that is, the control function need not be negative definite if all n determinants are negative. Negative definite-ness can be established by proving that $-H$ is positive definite.

Harmonic Control Functions: The harmonic constraint requires that the trace of the Hessian (or Laplacian) is identically zero:

$$\nabla^2 F = \frac{\partial^2 F}{\partial \theta_0^2} + \frac{\partial^2 F}{\partial \theta_1^2} + \cdots + \frac{\partial^2 F}{\partial \theta_n^2} = 0.$$

This constraint also produces a class of admissible control surfaces[11] and is similarly closed under linear composition. However, the equality constraint suggests that physically derived performance metrics that meet this criteria are rare.

Sub-Harmonic Control Functions: As the name suggests, sub-harmonic functions are closely related to harmonic functions. This class of admissible controllers requires the Laplacian to be less than or equal to zero:

$$\nabla^2 F = \frac{\partial^2 F}{\partial \theta_0^2} + \frac{\partial^2 F}{\partial \theta_1^2} + \cdots + \frac{\partial^2 F}{\partial \theta_n^2} \leq 0.$$

Once again, this form of control surface is closed under linear composition. The inequality constraint permits local maxima in a function with a single, global minimum. This suggests that there will be additional (unstable) singular points in the surface — but more important, there will be regions of the surface that are inaccessible due to local upward pointing gradients. This fact could have an unfortunate effect on the *completeness* properties of an admissible control function. Completeness requires that if a path to the goal exists, then there will be a gradient in all states of the system that lead to the goal[4]. The

[4]There are problems in practice related to numerical precision which we will not deal with here.

spurious *bubbles* in the state space allowed in the sub-harmonic constraint means that it may be possible that sub-harmonic functions cannot be proven complete.

All of these Hessian-based constraints on the control function, $F(\Theta)$, are closed under linear composition. Consider two control functions, F_1 and F_2. If both F_1 and F_2 are convex control surfaces, i.e., they exhibit positive definite Hessian matrices, then a linear combination, $c_1F_1 + c_2F_2$ will also yield a positive definite Hessian provided that c_1 and c_2 are both positive, since $c_1\partial^2F_1/\partial\Theta^2 + c_2\partial^2F_2/\partial\Theta^2$ must also be positive definite. The same reasoning applies to harmonic and sub-harmonic functions as well.

A.2 Planar Force Closure Sufficiency Metric Hessian

Planar grasping is much easier than the general 3D case! The force closure wrench model (Equation 16) simplifies to:

$$\begin{aligned} w_1 &= f_x = -cos(\theta) \\ w_2 &= f_y = -sin(\theta) \\ w_3 &= m_z = 0. \end{aligned}$$

This leads to the residual vector:

$$\vec{\rho} = \vec{t} - \frac{1}{n}\sum_i \vec{w}_i = \begin{bmatrix} t_{fx} - \frac{1}{n}\sum_i(-cos(\theta_i)) \\ t_{fy} - \frac{1}{n}\sum_i(-sin(\theta_i)) \\ t_{mz} \end{bmatrix} \tag{44}$$

and:

$$G_{\theta,i} = \begin{bmatrix} sin(\theta_i) \\ -cos(\theta_i) \\ 0 \end{bmatrix} \qquad \frac{\partial G_{\theta,i}}{\partial \theta_i} = \begin{bmatrix} cos(\theta_i) \\ sin(\theta_i) \\ 0 \end{bmatrix}$$

Therefore the diagonal terms in the Hessian look like:

$$\frac{\partial^2\epsilon}{\partial\theta_k^2} = \frac{2}{n}\left(\frac{G_k^TG_k}{n} - \frac{\partial G_k^T}{\partial\theta_k}\vec{\rho}\right) = \frac{1}{n} - (t_{fx} - \frac{1}{n}\sum_i -cos(\theta_i))cos(\theta_k) - (t_{fy} - \frac{1}{n}\sum_i -sin(\theta_i))sin(\theta_k)$$

and the off-diagonal terms look like:

$$\frac{\partial^2\epsilon}{\partial\theta_j\partial\theta_k} = \frac{2}{n^2}G_j^TG_k = \frac{2}{n^2}\left(sin(\theta_j)sin(\theta_k) + cos(\theta_j)cos(\theta_k)\right).$$

This Hessian is difficult to analyze in general, but if we consider two contacts when the external bias wrench, $\vec{t} = \vec{0}$, the Hessian becomes:

$$\frac{\partial^2\epsilon}{\partial\vec{\theta}^2} = \begin{bmatrix} -cos(\theta_1 - \theta_2) & cos(\theta_1 - \theta_2) \\ cos(\theta_1 - \theta_2) & -cos(\theta_1 - \theta_2) \end{bmatrix}. \tag{45}$$

Sylvesters theorem requires:

$$-cos(\theta_1 - \theta_2) > 0, and \tag{46}$$

$$\begin{vmatrix} -cos(\theta_1 - \theta_2) & cos(\theta_1 - \theta_2) \\ cos(\theta_1 - \theta_2) & -cos(\theta_1 - \theta_2) \end{vmatrix} > 0. \tag{47}$$

The first condition is satisfied when $\pi/2 \leq (\theta_1 - \theta_2) \leq 3\pi/2$. The determinant of the Hessian is identically zero. The Hessian is, therefore, positive semi-definite in this interval (with a single positive eigenvalue). This result is illustrated in Figure 3.

B A Quadratic Regulator for Unimodal Metric Spaces

Given the metric evaluated for the current configuration, and the metric evaluated at the optimal configuration,

$$\begin{aligned} \epsilon_S &= \epsilon_S(\theta_k) \\ \epsilon_S^* &= \epsilon_S(\theta_k^*), \end{aligned}$$

and requiring the gradient to vanish at the minimum,

$$\left.\frac{\partial \epsilon_S}{\partial \theta_k}\right|_{\theta_k^*} = 0,$$

we may solve for the coefficients of a quadratic control surface with the same properties.

Consider,

$$f(\theta) = a\theta^2 + b\theta + c,$$

the conditions enumerated above require:

$$\begin{aligned} f(\theta_k) &= a\theta_k^2 + b\theta_k + c = \epsilon_S \\ f(\theta_k^*) &= a\theta_k^{*2} + b\theta_k^* + c = \epsilon_S^* \\ f'(\theta_k^*) &= 2a\theta_k^* + b = 0. \end{aligned}$$

This set of three equations and three unknowns yields:

$$a = (\epsilon_S - \epsilon_S^*)/(\theta_k - \theta_k^*)^2 \quad (48)$$

$$b = -2a\theta_k^* \quad (49)$$

$$c = \epsilon_S^* + a\theta_k^{*2} \quad (50)$$

Therefore, the quadrtatic fit to the sufficiency metric for contact k becomes:

$$f(\theta) = \frac{\epsilon_S - \epsilon_S^*}{(\theta_k - \theta_k^*)^2}(\theta - \theta_k^*) + \epsilon_S^* \quad (51)$$

C Kinematics of the Utah/MIT Dextrous Hand

Figure 16 describes the kinematics of the Utah/MIT finger. For this coordinate system, the forward kinematics of the finger are given Equation 52.

$$\begin{aligned} x &= [l_0 sin(\phi) + l_1 sin(\theta_1 + \phi) + l_2 sin(\theta_1 + \theta_2 + \phi) + l_3 sin(\theta_1 + \theta_2 + \theta_3 + \phi)]\ sin(\theta_0) \\ y &= l_0 cos(\phi) + l_1 cos(\theta_1 + \phi) + l_2 cos(\theta_1 + \theta_2 + \phi) + l_3 cos(\theta_1 + \theta_2 + \theta_3 + \phi) \\ z &= [l_0 sin(\phi) + l_1 sin(\theta_1 + \phi) + l_2 sin(\theta_1 + \theta_2 + \phi) + l_3 sin(\theta_1 + \theta_2 + \theta_3 + \phi)]\ cos(\theta_0) \end{aligned} \quad (52)$$

The Jacobian for the finger geometry illustrated in Figure 16 is defined by Equation 53.

$$J = \begin{bmatrix} [l_0 s\phi + l_1 s1\phi + l_2 s12\phi + l_3 s123\phi]\, c0 & [l_1 c1\phi + l_2 c12\phi + l_3 c123\phi]\, s0 & [l_2 c12\phi + l_3 c123\phi]\, s0 & [l_3 c123\phi]\, s0 \\ 0 & -l_1 s1\phi - l_2 s12\phi - l_3 s123\phi & -l_2 s12\phi - l_3 s123\phi & -l_3 s123\phi \\ [l_0 s\phi + l_1 s1\phi + l_2 s12\phi + l_3 s123\phi]\, -s0 & [l_1 c1\phi + l_2 c12\phi + l_3 c123\phi]\, c0 & [l_2 c12\phi + l_3 c123\phi]\, c0 & [l_3 c123\phi]\, c0 \end{bmatrix} \quad (53)$$

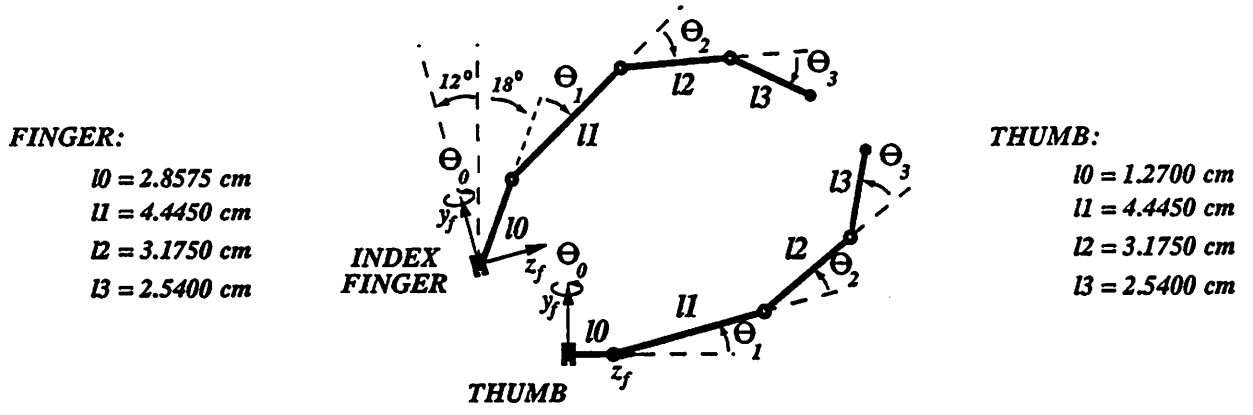

Figure 16: The Utah/MIT Finger/Thumb Geometry

where:

$$\begin{aligned} \phi &= 0.5236\ rad\ (30\ degrees), \\ cijk\phi &= cos(\theta_i + \theta_j + \theta_k + \phi),\ and \\ sijk\phi &= sin(\theta_i + \theta_j + \theta_k + \phi). \end{aligned}$$

The forward kinematics of the thumb are given Equation 54.

$$\begin{aligned} x &= [l_0 + l_1 cos(\theta_1) + l_2 cos(\theta_1 + \theta_2) + l_3 cos(\theta_1 + \theta_2 + \theta_3)]\ sin(\theta_0) \\ y &= l_1 sin(\theta_1) + l_2 sin(\theta_1 + \theta_2) + l_3 sin(\theta_1 + \theta_2 + \theta_3) \\ z &= [l_0 + l_1 cos(\theta_1) + l_2 cos(\theta_1 + \theta_2) + l_3 cos(\theta_1 + \theta_2 + \theta_3)]\ cos(\theta_0) \end{aligned} \tag{54}$$

The Jacobian for the thumb is expressed by Equation 55.

$$J = \begin{bmatrix} [l_0 + l_1 c1 + l_2 c12 + l_3 c123]\, c0 & [-l_1 s1 - l_2 s12 - l_3 s123]\, s0 & [-l_2 s12 - l_3 s123]\, s0 & [-l_3 s123]\, s0 \\ 0 & l_1 c1 + l_2 c12 + l_3 c123 & l_2 c12 + l_3 c123 & l_3 c123 \\ [l_0 + l_1 c1 + l_2 c12 + l_3 c123]\, -s0 & [-l_1 s1 - l_2 s12 - l_3 s123]\, c0 & [-l_2 s12 - l_3 s123]\, c0 & [-l_3 s123]\, c0 \end{bmatrix} \tag{55}$$

D Parametric Decision Surfaces - Luce's Rule

The switching "boundary" is, by convention, the locus of points in this continuous activation function where, $A_0 = A_1 = \cdots = A_n = 1/(n+1)$. The γ are computed using the parameters $(\kappa_i, \kappa_j, \beta_{ij})$ illustrated in Figure 17. For two competing behaviors, the switching boundary is defined as the locus of points in the error plane where competitive behaviors are equally activated, i.e., $A_0 = A_1 = 1/2$, or equivalently:

$$\begin{aligned} e^{k_0 \epsilon_0 + b_0} &= e^{k_1 \epsilon_1 + b_1},\ or \\ k_0 \epsilon_0 + b_0 &= k_1 \epsilon_1 + b_1,\ and \end{aligned}$$

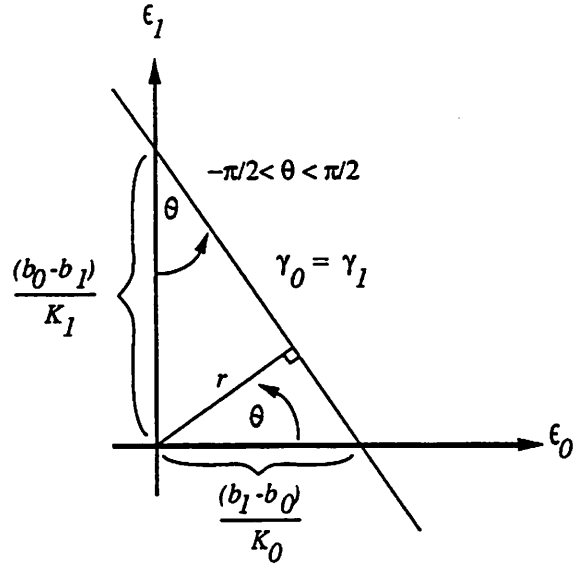

$$\gamma_0 = K_0\epsilon_0 + b_0$$

$$\gamma_1 = K_1\epsilon_1 + b_1$$

relative strength:
K_0 , K_1

bias:
$b_0 = - b_1$

Figure 17: The Parametric Switching Surface

$$\epsilon_0 = \frac{k_1}{k_0}\epsilon_1 + \frac{(b_1 - b_0)}{k_0}$$
$$\epsilon_1 = \frac{k_0}{k_1}\epsilon_0 + \frac{(b_0 - b_1)}{k_1}$$

The slope/intercept form of the switching boundary defines the ϵ_0 and ϵ_1 intercepts illustrated in Figure 17. This geometry yields:

$$tan(\theta) = -\frac{K_1}{K_0}$$

or equivalently,

$$sin(\theta) = rK_1/(b_0 - b_1) = rK_1/(2b_0) \quad (56)$$
$$cos(\theta) = rK_0/(b_1 - b_0) = rK_0/(-2b_0) \quad (57)$$

The switching profile is modulated by controlling the gradient magnitude, σ, at the switch boundary.

$$\sigma^2 = |\nabla A_0| = \left[\frac{\partial A_0}{\partial \epsilon_0}^2 + \frac{\partial A_0}{\partial \epsilon_1}^2\right] \quad (58)$$

By convention, we have selected the negative root of Equation 58 so that activation A_0 increases in the $\hat{r}$ direction.

$$A_0 = \frac{e^{(K_0\epsilon_0 + b_0)}}{e^{(K_0\epsilon_0 + b_0)} + e^{(K_1\epsilon_1 + b_1)}} \quad (59)$$

Differentiating A_0 with respect to ϵ_0 and ϵ_1 yields:

$$\frac{\partial A_0}{\partial \epsilon_0} = \frac{K_0 e^{(K_0\epsilon_0 + b_0)} e^{(K_1\epsilon_1 + b_1)}}{\left[e^{(K_0\epsilon_0 + b_0)} + e^{(K_1\epsilon_1 + b_1)}\right]^2} \quad (60)$$

$$= K_0 A_0 A_1 \tag{61}$$

$$\frac{\partial A_0}{\partial \epsilon_1} = \frac{-K_1 e^{(K_0\epsilon_0+b_0)} e^{(K_1\epsilon_1+b_1)}}{\left[e^{(K_0\epsilon_0+b_0)} + e^{(K_1\epsilon_1+b_1)}\right]^2} \tag{62}$$

$$= -K_1 A_0 A_1. \tag{63}$$

Therefore,

$$\|\nabla A_0\| = -A_0 A_1 \left[K_0^2 + K_1^2\right]^{1/2}$$

and σ is computed by evaluating this gradient on the switching boundary where, $A_0 = A_1 = 1/2$,

$$\sigma = |\nabla A_0|_{boundary} = \frac{-(K_0^2 + K_1^2)^{1/2}}{4}. \tag{64}$$

Now,

$$\begin{aligned} Eqn\ 64 &\implies (K_0^2 + K_1^2)^{1/2} = -4\sigma \\ Eqn\ 56 &\implies K_1 = 2b_0/r sin(\theta) \\ Eqn\ 57 &\implies K_0 = -2b_0/r cos(\theta). \end{aligned}$$

Therefore,

$$\left(\frac{4b_0^2}{r^2} cos^2(\theta) + \frac{4b_0^2}{r^2} sin^2(\theta)\right)^{1/2} = -4\sigma$$

And finally,

$$\begin{aligned} b_0 &= -2r\sigma \\ K_0 &= -\frac{2b_0}{r} cos(\theta) = 4\sigma cos(\theta) \\ K_1 &= \frac{2b_0}{r} sin(\theta) = -4\sigma sin(\theta) \end{aligned}$$

Figures 18, 19, and 20 illustrate the effect of these parameters on the decision surface in the error space.

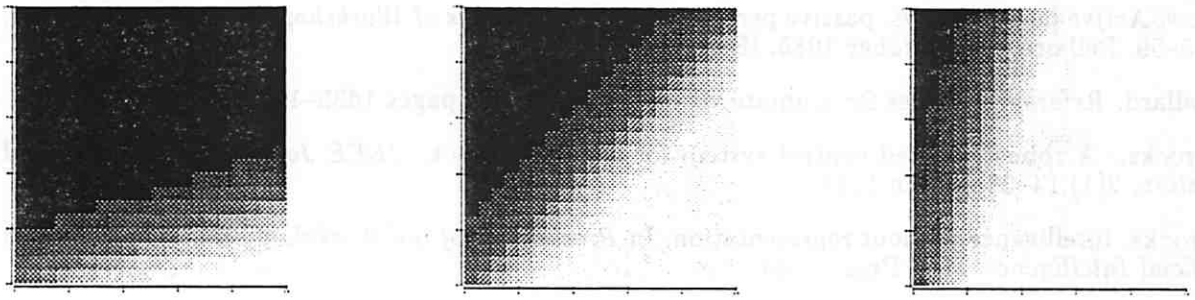

Figure 18: Influence of θ over the decision surface ($r = 0.0, \sigma = 0.5$)

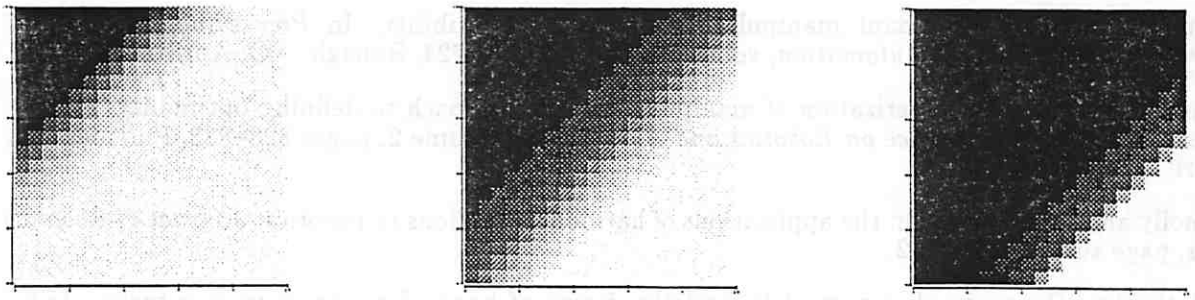

Figure 19: Influence of r over the decision surface ($\theta = -\pi/4$, $\sigma = 0.5$)

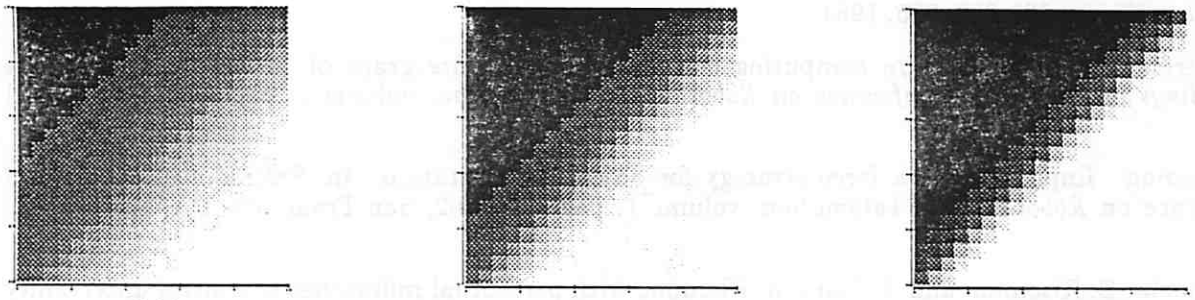

Figure 20: Influence of σ over the decision surface ($\theta == -\pi/4$, $r = 0.0$)

References

[1] P.K. Allen. Surface descriptions from vision and touch. In *Proceedings of the 1984 Conference on Robotics*, pages 394–397, Atlanta, GA, March 1984. IEEE.

[2] P.K. Allen. Sensing and describing 3-d structure. In *Proceedings of the 1986 Conference on Robotics and Automation*, volume 1, pages 126–131, San Francisco, CA, April 1986. IEEE.

[3] R. Bajcsy. Active perception vs. passive perception. In *Proceedings of Workshop on Computer Vision*, pages 55–59, Bellaire, MI, October 1985. IEEE.

[4] D.H. Ballard. Reference frames for animate vision. In *IJCAI-89*, pages 1635–1641, August 1989.

[5] R.A. Brooks. A robust layered control system for a mobile robot. *IEEE Journal of Robotics and Automation*, 2(1):14–23, March 1986.

[6] R.A. Brooks. Intelligence without representation. In *Proceedings of the Workshop on the Foundations of Artificial Intelligence*. MIT Press, 1987.

[7] J.S. Bruner. Organization of early skilled action. *Child Development*, 44:1–11, 1973.

[8] J.F. Canny. *The Complexity of Robot Motion Planning*. MIT Press, Cambridge, MA, 1988.

[9] S.L. Chiu. Control of redundant manipulators for task compatibility. In *Proceedings of the 1987 Conference on Robotics and Automation*, volume 3, pages 1718–1724, Raleigh, NC, April 1987. IEEE.

[10] S.L. Chiu. Kinematic characterization of manipulators: An approach to defining optimality. In *Proceedings of the 1988 Conference on Robotics and Automation*, volume 2, pages 828–833, Philadelphia, PA, April 1988. IEEE.

[11] C. Connolly and R. Grupen. On the applications of harmonic functions to robotics. *Journal of Robotics Systems*, page submitted, 1992.

[12] M.R. Cutkosky. On grasp choice, models, and the design of hands for manufacturing tasks. *IEEE Transactions on Robotics and Automation*, 5(3):269–279, June 1989.

[13] R.E. Ellis. Extraction of tactile features by passive and active sensing. *SPIE Intelligent Robots and Computer Vision*, 521:289–295, 1984.

[14] B. Faverjon and J. Ponce. On computing two-finger force-closure graps of curved 2d objects. In *Proceedings of the IEEE Conference on Robotics and Automation*, volume 1, pages 424–429, April 1991.

[15] R.S. Fearing. Implementing a force strategy for object re-orientation. In *Proceedings of the 1986 Conference on Robotics and Automation*, volume 1, pages 96–102, San Francisco, CA, April 1986. IEEE.

[16] C. Fennema, E. Riseman, and A. Hanson. Planning with perceptual milestones to control uncertainty in robot navigation. In *Proc. of SPIE*, pages 1–16, Cambridge, November 1988. International Society for Photographic and Industrial Engineering.

[17] G.H. Golub and C.F. Van Loan. *Matrix Computations*. The Johns Hopkins University Press, Baltimore, MD, 1983.

[18] W.E.L. Grimson and T. Lozano-Pérez. Model-based recognition and localization from tactile data. *Journal of Robotics Research*, 3(3):3–35, 1986.

[19] R.A. Grupen. *General Purpose Grasping and Manipulation with Multifingered Robot Hands*. PhD thesis, University of Utah, Merrill Engineering Building, Salt Lake City, UT 84112, August 1988.

[20] R.A. Grupen, K. Biggers, T.C. Henderson, and S. Meek. Task defined internal grasp wrenches. Technical Report UUCS-88-001, Department of Computer Science, University of Utah, 1988.

[21] R.A. Grupen and R.S. Weiss. Sensor-based planning for grasping and manipulation with multifingered robot hands. Technical Report COINS Technical Report 90-58, COINS Department, University of Massachusetts, July 1990.

[22] V. Gullapalli, R. Grupen, and A. Barto. Learning reactive admittance control. In *Proceedings of the 1992 Conference on Robotics and Automation*, pages 1475–1480, Nice, FRANCE, May 1992. IEEE.

[23] S. Hutchinson and A. Kak. Planning sensing strategies in a robot work cell with multi-sensor capabilities. *IEEE Transactions on Robotics and Automation*, 5(6):765–783, 1989.

[24] T. Iberall. Grasp planning for human prehension. In *Proceedings of the International Joint Conference on Artificial Intelligence*, pages 1153–1156, 1987.

[25] J.W. Jameson and L.J. Leifer. Automatic grasping: An optimization approach. *IEEE Transactions on Systems, Man, and Cybernetics*, SMC-17(5):806–814, September 1987.

[26] J. Kerr and B. Roth. Analysis of multifingered hands. *Journal of Robotics Research*, 4(4):3–17, Winter 1986.

[27] C. Klein and B. Blaho. Dexterity measures for the design and control of kinematically redundant manipulators. *Journal of Robotics Research*, 6(2):72–83, Summer 1987.

[28] Z. Li, P. Hsu, and S. Sastry. Grasping and coordinated manipulation by a multifingered robot hand. *International Journal of Robotics Research*, 8(4):33–50, August 1989.

[29] Z. Li and S. Sastry. Task-oriented optimal grasping by multifingered robot hands. *IEEE Journal of Robotics and Automation*, 4(1):32–44, February 1988.

[30] Z. Li and S. Sastry. Task-oriented optimal grasping by multifingered robot hands. *IEEE Transactions Systems, Man, and Cybernetics*, 11(10):681–689, 1988.

[31] M.T. Mason. *Manipulator Grasping and Pushing Operations.* PhD thesis, Massachusetts Institute of Technology, Cambridge, Mass, June 1982.

[32] M.T. Mason and J.K. Salisbury. *Robot Hands and the Mechanics of Manipulation.* The MIT Press, Cambridge, MA, 1985.

[33] Y. Nakamura and H. Hanafusa. Optimal redundancy control of robot manipulators. *Journal of Robotics Research*, 6(1), Spring 1987.

[34] Y. Nakamura, K. Nagai, and T. Yoshikawa. Mechanics of coordinated manipulation by multiple robotic mechanisms. In *Proceedings of the 1987 Conference on Robotics and Automation*, volume 2, pages 991–998, Raleigh, NC, April 1987. IEEE.

[35] T.N. Nguyen and H.E. Stephanou. A topological algorithm for continuous grasp planning. In *Proceeding of the 1990 IEEE Conference on Robotics and Automation*, pages 670–675, Cincinatti, OH, 1990. IEEE.

[36] V.D. Nguyen. Constructing force closure grasps. *International Journal of Robotics Research*, 7(3):3–16, 1988.

[37] V.D. Nguyen. Constructing stable grasps. *International Journal of Robotics Research*, 8(1):26–37, 1989.

[38] M.H. Raibert. *Legged Robots that Balance.* MIT Press, Cambridge, MA, 1986.

[39] J.K. Salisbury. *Kinematic and Force Analysis of Articulated Hands.* PhD thesis, Stanford University, May 1982.

[40] J.T. Schwartz, M. Shahir, and J. Hopcroft, editors. *Planning, Geometry and Complexity of Robot Motion.* Ablex Publishing Corporation, Norwood, New Jersey, 1987.

[41] K. Shaw and R.A. Grupen. Parallel stiffness controller for the stanford/jpl hand. Technical Report COINS Technical Report 90-48, COINS Department, University of Massachusetts, June 1990.

[42] A. Shmuel and M. Werman. Active vision: 3d from an image sequence. In *Proceedings of the International Conference on Pattern Recognition*, pages 48–53, June 1990.

[43] E. Thelen, D. Corbetta, K. Kamm, J. Spencer, K. Schneider, and R. Zernicke. The transition to reaching: Mapping intention and intrinsic dynamics. *Unpublished*, 1992.

[44] R. Tomovic, G. Bekey, and W. Karplus. A strategy for grasp synthesis with multifingered robot hands. In *Proceedings of the 1987 Conference on Robotics and Automation*, pages 83–89, Raleigh, NC, April 1987. IEEE.

[45] J.C. Trinkle and R.P. Paul. The initial grasp liftability chart. *IEEE Journal of Robotics and Automation*, 5(1):47–52, February 1989.

[46] L. Whitcomb, D. Koditschek, and J. Cabrera. Toward the automatic control of robot assembly tasks via potential functions: The case of 2-d sphere assemblies. In *Proceedings of the 1992 Conference on Robotics and Automation*, volume 3, pages 2186–2191, Nice, FRANCE, May 1992. IEEE.

[47] T. Yoshikawa. Analysis and control of robot manipulators with redundancy. In *Robotics Research: The First International Symposium*, pages 735–747, 1984.

[48] T. Yoshikawa. Manipulability of robotic mechanisms. *Journal of Robotics Research*, 4(2):3–9, Summer 1985.